Revision 1 Word Count:16709

Interfacial Interactions Controlling Adsorption of Metal Cations onto Montmorillonites

Ke Jin Li[a,b,1], Alfin Kurniawan[a,b,1], Georgios E. Christidis[c], Jia Yong He[a,b], and Chun Hui Zhou[a,b,*]

[a] Research Group for Advanced Materials & Sustainable Catalysis (AMSC), State Key Laboratory Breeding Base of Green Chemistry-Synthesis Technology, College of Chemical Engineering, Zhejiang University of Technology, Hangzhou 310032, China. E-mail: clay@zjut.edu.cn

[b] Qing Yang Institute for Industrial Minerals (QYIM), You Hua, Qing Yang, Chi Zhou 242804, China

[c] School of Mineral Resources Engineering, Technical University of Crete, 73100 Chania, Greece

[1] These authors contributed equally to this work

Abstract

Montmorillonite (Mt) is a ubiquitous swelling clay mineral and major solid-phase component of rocks, sediments, and soils with excellent capability of adsorbing metal cations. This unique feature renders Mt important for the enrichment and mobilization of environmentally important metal cations, the evolution of Mt itself, soils and related sediments during, and other geological processes. However, the interfacial interactions of Mt during adsorption of metal cations at the molecular level remain rather elusive, due to the chemical and structural complexity of Mt surfaces and the diverse properties of metal cations. Herein, we provide a comprehensive review of the adsorption modes of metal cations on basal and edge surfaces of Mt, local chemical environments of adsorption sites, the driving forces governing metal sorption behavior, and key factors influencing the dynamics of cation uptake. Various surface complexation models (i.e., NEM, CCM, DLM,

and TLM), advanced spectroscopic techniques (i.e., EXAFS, XANES, TRLFS, and NMR), and atomistic simulation methods (i.e., MD, DFT, and FPMD) have been applied in conjunction with macroscopic adsorption experiments to gain detailed insights into the interfacial interactions of metal cations on Mt. Mt adsorbs metal cations via three independent pathways: (i) cation exchange; (ii) surface complexation, and (iii) nucleation and surface precipitation. The main driving force for cation exchange is electrostatic interaction while chemical bonding is the driving force for the other two pathways that depend on the basal and edge surface properties of Mt. The siloxane cavities on the tetrahedral basal plane exhibit the strongest adsorption sites for cation exchange and are greatly affected by the Al^{3+}/Si^{4+} tetrahedral substitutions. At amphoteric edge surfaces bearing hydroxyl groups, metal cations form mono/multidentate surface complexes on Mt [010] and [110] edges. Ionic strength, pH, the presence of competing cations, temperature, and layer charge have been shown to be the main parameters influencing the adsorption mechanisms and quantity of adsorbed cations. The up-to-date knowledge of interfacial interactions between metal cations and Mt basal and edge surfaces presented in this Review provides a better understanding of the enrichment of metals, formation of metal ores, and natural biogeochemical cycles, as well as may widen the applications of layered clay minerals in environmental remediation, radioactive waste repositories, petroleum exploration and extraction, and extraterrestrial research.

Keywords: Montmorillonite; Interfacial interaction; Adsorption; Metal cation; Cation exchange; Surface complexation; Precipitation

1. Introduction

Montmorillonite (Mt), with an ideal unit cell formula of $M^{+}_{y}[Si_8][Al_{4-y}Mg]O_{20}(OH)_4$, is a layered aluminosilicate material found ubiquitously in terrestrial and marine environments, being the fine-grained fraction of rocks, sediments, and soils (Anderson et al., 2010; Zhu et al., 2016). Considering its large surface area, thermal and mechanical stability, and intrinsically high cation exchange capacity, Mt has proven to be an efficient cation adsorbent and plays an important role in Earth's geological cycles, environmental protection, and various industrial processes (see **Fig. 1A**). In particular, adsorption of metal cations onto Mt is a key process governing the enrichment and migration of metals in soils and rocks, illitization process of Mt during diagenesis, formation of metal ores, and the natural biogeochemical cycles (Sposito et al., 1999; Tournassat et al., 2011; Zhang et al., 2019b; Liu et al., 2022). From a practical environmental application point of view, Mt has been widely employed as an efficient and low-cost adsorbent for removing various harmful metal cations, such as radionuclides (e.g., $[UO_2]^{2+}$, $^{137}Cs^{+}$, $^{90}Sr^{2+}$, and $^{60}Co^{2+}$) and non-radioactive (e.g., Pb^{2+}, Hg^{2+}, Cd^{2+}, and Tl^{+}) heavy metals from fertilizers, industrial wastes, ore mining, sewage sludges, and the water and soil in the vicinity of mines and nuclear waste storage sites (Halim et al., 2003; Uddin, 2017; Zhang et al., 2018b; Balali-Mood et al., 2021; Voegelin et al., 2022). Interactions of metal cations with Mt surface are also great importance in applications, such as design of engineered containment barriers in nuclear waste management, drilling muds during oil extraction, and catalysis reactions (Anderson et al., 2010; Payne et al., 2013; Huang et al., 2021). Therefore, the interfacial interaction for the adsorption of cations on Mt have significant implications for and environmental fields. While most previous studies focus mainly on

the improvement of cation adsorption performance of Mt via physical and chemical modifications, much less efforts attempt to understand the modes of interaction between cations and Mt surfaces at the molecular level.

The remarkable adsorption of Mt for metal cations arises from its unique layer structure and surface charge heterogeneity. As a 2:1 phyllosilicate mineral, Mt lattice consists of a sandwiched assembly of one AlO_6 octahedral and two SiO_4 tetrahedral sheets, forming the so-called "T-O-T" (tetrahedral-octahedral-tetrahedral) layer type (**Fig. 1B**) (Guggenheim et al., 2006). Natural Mt commonly possesses a *cis*-vacant T-O-T layer comprising both *cis*- (OH groups on adjacent corners) and *trans*-octahedra (OH groups on opposite corners) within the octahedral sheet (Gao et al., 2023). This expandable layered structure affords plentiful adsorption sites on Mt where cations can be accommodated in the external, internal, and edge surfaces. The isomorphic substitutions of cations in the octahedral (e.g., Mg^{2+} or Fe^{2+} for Al^{3+}) and tetrahedral sheets (e.g., Al^{3+} for Si^{4+}) of Mt generate negative charges on faces, which are compensated by the adsorbed metal cations through cation exchange. In addition to the negatively charged basal plane surface, the presence of abundant reactive hydroxyl groups (≡SOH) on the edge and defects endows Mt with strong capability to sorb metal cations by surface complexation and nucleation/surface precipitation reactions (Balasubramanian et al., 2009; de Pablo et al., 2011; Schindler et al., 2015; Ozsoy and Bekbolet, 2018).

Studies of metal cation adsorption on Mt have been documented in the literature as early as a century ago, with research are still undergoing to gain deeper insights into the Mt–cation interface interactions with molecular-level detail for the design of adsorbent and other functional materials. In order to understand and predict adsorption behavior of

95 cations onto Mt surfaces, batch adsorption experiments have often been performed under
96 different conditions, such as pH, ionic strength, solid/liquid (S/L) ratio, and initial
97 concentration. For practical applications, the obtained adsorption edges (pH function) and
98 isotherm data (concentrations) are fitted with either empirical or thermodynamic
99 (mechanistic) models. In the latter context, the diffuse layer model (DLM), triple layer
100 model (TLM), constant capacitance model (CCM), nonelectrostatic model (NEM), and

N

Li et al., 2021b). According to the classic hybrid orbital theory, the formation of stable covalent bonds between metal cations and oxygen atoms of Mt basal surface is unlikely, because of the low energy of lone-pair electrons of surface oxygen atoms. However, according to the quantum mechanical analysis, in such a strong electric field, the atom/cation structure near charged interfaces can be substantially changed. In particular, the polarizabilities of atom/cation are significantly larger than the classical polarizability values under strong electric field of Mt surface (Liu et al., 2019). In terms of the O atoms on Mt basal surface or metal cations, the outer-shell n*s* and np_z orbitals can be hybridized to form n*s*np_{z+} and n*s*np_{z-} orbitals (n = 2, 3), respectively, leading to the adsorption of cations on Mt basal surface through non-classical polarization-induced covalent bonding (Liu et al., 2014b; Liu et al., 2019; Li et al., 2019a, 2021a, 2021b). This non-classical polarization-induced force is regarded to be strong as a covalent bonding force.

4. Interfacial interactions of metal cations with the edge surfaces

4.1 Surface Complexation

While cation exchange is considered to be the predominant mechanism that controls metal adsorption on the surface basal plane of Mt, surface complexation plays a major role in metal retention at edge surfaces. As mentioned earlier, Mt particles possess hydroxyl functionality at the edge sites and related defects, though the amount is relatively low, which may dominate the adsorption process, especially under the conditions of high ionic strength, high pH, or trace concentrations of metal cations (Manning and Goldberg, 1997; Schlegel and Manceau, 2006; Gu et al., 2010; Tournassat et al., 2013). The edge surface area ($a_{s,edge}$) of Mt calculated by atomic force microscopy (AFM) and MD simulations is about 4.3 ± 0.2 m^2 g^{-1}, while the edges perpendicular to the

[110] and [010] crystal planes, also called as AC and B edges, account for about 60 and 20% of total edge surface, respectively (Kraevsky et al. 2020). These AC and B sites are considered to be the most stable edge surfaces of Mt (Newton and Sposito, 2015; Kwon and Newton, 2016; Newton et al., 2016) and have been demonstrated to be unaffected by temperature. In addition, the AC edge exhibits higher chemical stability in an aqueous solution than the B edge (Kwon and Newton, 2016), due to the presence of hydroyxl groups for the complexation of the process.

Metal cations are mainly adsorbed onto the AC and B edges of Mt. When there are no isomorphic substitutions in the crystal lattice of Mt, ≡Si-OH/≡Al-OH_2 and ≡Si-OH/≡Al-OH_2/≡(SiAl)OH are the main groups present on the Mt edge that are perpendicular to the [010] and [110] planes, respectively (Tournassat et al., 2016). The acid–base chemistry of ≡Si-OH/≡Al-OH_2/≡(SiAl)OH is essential to the surface reactivity of Mt edges. In this regard, the accurate determination of the intrinsic pK_a values is important as they not only describe the acid–base properties of Mt edge sites, but also serve as a critical parameter for the adsorption modeling. However, the reported pK_a values of Mt edge surface sites obtained from potentiometric titration experiments, valence bond theories, and atomistic MD simulations (i.e., AIMD and FPMD) vary widely among previous studies (Bickmore et al., 2003; Tournassat et al., 2004; Liu et al., 2013a, 2014a). Currently, the structures of the AC and B edge surfaces and the associated pK_a values predicted by *ab initio* MD (AIMD) simulations are considered the most accurate (**Fig. 4**). The pK_a values of the edge sites without tetrahedral or octahedral substitutions range from 5 to 8, indicating that these sites are readily deprotonated at higher pH values and thus act as effective metal complexing sites. On the other hand,

very high pK_a values have been reported for edge surfaces with isomorphic substitutions, i.e., ≡AlOH on the tetrahedral sheet (pK_a = 15.1) and ≡$Mg(OH)_2$, ≡$Fe(OH)_2$ on the octahedral sheet (pK_a = 13.2), and thus these structural OH groups do not show reactivity at common pH. Moreover, the pK_a values of Mt edge sites are not significantly changed, especially at low temperatures below 353 K (Duc et al., 2008; Liu et al., 2015). However, with increasing temperature, the acidity of edge sites gradually increases, suggesting that the edge surfaces have more complex sites to adsorb metal cations (Liu et al., 2015).

Numerous batch adsorption experiments and modeling studies have demonstrated that there exists two types of adsorption sites on Mt edges, the so-called strong sites (≡ S^SOH) with high affinity but limited adsorption capacity (~2 mmol/kg) and weak sites (≡ S^WOH) possessing high capacity (~40 mmol/kg) sites but weak adsorptivity (Bradbury and Baeyens, 1997; Baeyens B and Bradbury, 2002; Marques Fernandes et al., 2016). Still, challenges remain to more comprehensively understand the interfacial interaction between metal cations and the edge adsorption sites at the molecular level, mainly due to the complexity of the crystal planes and the variability of surface functional groups. Toward addressing this understanding, various spectroscopic techniques, such as EXAFS, XANES, TRLFS, and NMR have been employed to investigate the interfacial interactions of heavy metal and radioactive cations on Mt edge surfaces. However, the above spectroscopic techniques have some limitations, such as (1) metal cations adsorbed on Mt edges require higher concentrations; (2) the structure of Mt edges should be well characterized and structure cannot be changed during experiment; (3) multiple complexes on Mt edges cannot be detected and differentiated individually (Liu et al., 2022). Thus, the spectroscopic investigations of the interfacial adsorption

interactions of metal cations on Mt are usually accompanied by atomistic computer simulations (i.e., MD, DFT, and FPMD).

The possible chemical environments of the adsorption sites on Mt edges are summarized in **Table 2**. Metal cations are adsorbed on the [010] and [110] edges and form monodentate/multidentate surface complexes. EXAFS studies revealed that Zn^{2+}, Ni^{2+} and Cu^{2+} ions were incorporated into the octahedron or formed inner-sphere complexes at Mt edges (Dähn et al., 2003, 2011; Churakov and Dähn, 2012; Schlegel and Manceau, 2013). More specifically, FPMD simulation indicated that Ni^{2+} cations formed tetradentate, bidentate and monodentate complexes on the octahedral vacant site, ≡$Al(OH)_2$/≡AlOH≡AlSiO and ≡SiOH sites on [010] or [110] edges, respectively (**Fig. 5A and B**) (Zhang et al., 2017). The tetradentate complex is significantly more stable than the monodentate and bidentate ones based on the computed desorption free energies (ΔF), indicating that the vacant site should be classified as the strong site while $Al(OH)_2$/ ≡AlOH≡AlSiO /≡SiOH are weak sites (Zhang et al., 2017). However, in the case of radioactive metal cations, e.g., adsorption of uranyl (UO_2^{2+}) on Mt edge surface, most studies suggested that both the Al octahedral and Si tetrahedral on Mt edge surfaces are possible binding sites and identified that bidentate complexes as the predominant surface species (**Fig. 5D**) (Hennig et al., 2002; Schlegel and Descostes, 2009; Marques Fernandes et al., 2012; Kremleva et al., 2015; Zhang et al., 2018b). The binding free energies for UO_2^{2+} complexes are very similar, hence these adsorption sites have similar affinity for UO_2^{2+} (Kremleva et al., 2015; Zhang et al., 2018b).

The adsorption behaviors of other divalent cations, such as Cd^{2+}, Cu^{2+}, Fe^{2+}, and Co^{2+} on Mt edges are similar to that of Ni^{2+}, in which all these metals were found to

preferentially adsorb onto the vacant sites than on the ≡SiOH, ≡$Al(OH)_2$, and ≡(AlSi)OH sites (Liu et al., 2014a, 2016, 2017, 2018a). In contrast, Pb^{2+} ions possess similar adsorption affinities toward the octahedral vacancy, ≡SiOH, ≡$Al(OH)_2$, or ≡(AlSi)OH sites (Zhang et al., 2019a). The reason for this difference in sorption behavior could be attributed to the chemical properties of metal cations itself, such as ionic radius. In this regard, Ni^{2+} (0.55 Å), Cd^{2+} (0.78 Å), Cu^{2+} (0.57 Å), Fe^{2+} (0.63 Å), and Co^{2+} (0.58 Å) all have relatively similar ionic radii, while the ionic radius of Pb^{2+} cation (0.98 Å) is notably larger than these cations. Thus, differences in the ionic radius of metal cations may account for this phenomenon. Moreover, cations having ionic radii smaller than Cd^{2+} are capable to enter the center of the vacant site, while those of the larger ones are adsorbed out of the center of the vacant site, thus leading to the difference in adsorption behaviors (**Fig. 5C**) (Zhang et al., 2017, 2019a). Similar volume effects appear on the complex adsorption of radioactive elements that usually exist in the form of metal oxide cations. Thus, the UO_2^{2+} cation with relatively large cross-sectional area that is adsorbed on Mt edge sites makes the adsorption at adjacent sites difficult (**Fig. 5D**) (Zhang et al., 2018b). By contrast, this phenomenon does not exist in the adsorption of transition metal cations at Mt edge surfaces (Zhang et al., 2018a, 2018b).

4.2 Nucleation and Surface Precipitation

At high pH values and solute concentrations, adsorption isotherms show that there is a distinct mode of metal uptake by Mt other than cation exchange and surface complexation, which is often referred to as nucleation and precipitation (Ford and Sparks, 2000; Schlegel and Manceau, 2006; Zhang et al., 2018a, 2018b, 2019a, 2019b). In this

441 regard, surface-induced nucleation and precipitation are often considered to be the main
442 mechanism for fixation and transport of heavy metal elements in nature. Common metal
443 cations that are adsorbed by precipitation include heavy metals (e.g., Zn^{2+}, Ni^{2+}, Co^{2+} and
444 Fe^{2+}) and radionuclides (e.g., Th^{+}, Tl, and U).

445 Due to the limitations of experimental techniques, most studies on the
446 precipitation-induced adsorption mainly focus on characterizing the adsorption
447 morphology. Very recently, the first-principles molecular dynamics (FPMD) technique
448 has been successfully applied to elucidate the detailed mechanism of surface
449 precipitation–adsorption, which revealed that the early stages of nucleation involve an
450 adsorption-hydrolysis-adsorption process. Specifically, water molecules coordinated to
451 metal cations adsorbed on Mt edge sites under ambient pH conditions can be further
452 deprotonated, forming hydroxyl groups that can serve as new binding sites for subsequent
453 adsorption. For example, while Ni^{2+} ions being able to accommodate $\equiv$SiOH, $\equiv$
454 $Al(OH)_2$, and the octahedral vacancy sites of Mt edges, only those adsorbed on the latter
455 site can undergo deprotonation at ambient conditions (Zhang et al., 2017). Hence, part of
456 Ni^{2+} ions can be adsorbed by nucleation and precipitation. On the other hand, the
457 adsorbed Pb^{2+} with extremely high pK_a values cannot generate new adsorption sites
458 (Zhang et al., 2019a). Further investigations under different conditions indicated that
459 there are two major pathways for nucleation and precipitation (Zhang et al., 2019b). One
460 is the stepwise route, where adsorbed metal cations on Mt edges firstly form metal
461 hydroxides that are subsequently converted into layer silicates upon reacting with silicon
462 (**Fig. 6A**). Another pathway is the synchronous route, in which the adsorption solution
463 initially contains dissolved Si, and thus metal cations and silicic acid could nucleate

directly onto Mt edges without preformation of metal hydroxides (**Fig. 6B**). Among these two pathways, the synchronous route is thermodynamically more favorable than the stepwise one, indicating that the nucleation process of metal cations on Mt edge surface prefers via synchronous route when dissolved Si is present.

5. Parameters affecting cation adsorption onto Mt surfaces

5.1 Ionic strength and pH

Ionic strength and pH are thought to be the two most important factors affecting the sorptive behavior of metal cations on Mt, as and have been widely studied in the past (Schultz and Grundl, 2004; Ozdemir and Yapar, 2009; Yu et al., 2016; Sugiura et al., 2021). As mentioned above, the edge surfaces of Mt exhibit a pH-dependent charging behavior associated with the protonation and deprotonation reactions of OH groups from unsatisfied bonds, which subsequently affect the efficiency and capacity of cation uptake. In this regard, metal cations bind to the Mt edge surfaces mainly in the form of OSSC at low pH values, whereas ISSC predominantly exists in near-neutral and alkaline pH conditions. With a further increase in pH, the adsorbed cations on the Mt edge surfaces could be deprotonated and become sites for the subsequent metal cations can be adsorbed onto this site, and removed by co-precipitation (**Fig. 7A**). At low pH values, the presence of abundant H^+ can act as competitive cations to compete with metal cations for the adsorption sites on Mt surface (Novikau and Lujaniene, 2022), resulting in a relatively small amount of adsorbed metal cations. In addition, pH profoundly affects the chemical composition of Mt adsorption sites, especially the edge hydroxyl groups, as well as the hydration forms and distribution of metal cations (**Fig. 7B**).

Ionic strength also modulates the sorptive behavior of metal cations on Mt, particularly more significant at low pH than at high pH. This implies that ionic strength affects cation exchange-based adsorption process. For example, batch adsorption experiments of Cd^{2+}, Cu^{2+}, Ni^{2+}, Pb^{2+}, and Zn^{2+} onto Mt at various pH and ionic strength conditions have been investigated (**Fig. 7C**) (Gu et al., 2010). The results showed that the uptake of these five cations was highly dependent on the ionic strength at low pH and the decrease of ionic strength would in turn lead to the increase of the relative proportion of cation exchange in the whole adsorption process. One possible explanation for this behavior could be attributed to the fact that the background electrolyte ions can compete with the target metal cations for exchange sites on the basal plane, while another one is related to the stacking states of Mt. With regard to the latter, it has been shown that ionic strength affects the orientation modes of asymmetric Mt platelets in aqueous suspensions. Specifically, Mt layers remain completely dispersed in the unsalted solution, while the association modes change from edge-to-edge to edge-to-face and to face-to-face orientation with the increase of ionic strength (**Fig. 7D**) (Gupt et al. 2020). Moreover, it is suggested that the face-to-face stacking of Mt lamellae at high salt concentrations would reduce the thickness of the diffuse double layer (DDL) and the adsorption area, thus leading to the decrease in adsorbed amount (Gupt et al. 2020). Besides, the cation exchange process is accompanied by the stratification and stacking of Mt layers (Whittaker et al. 2019) and it is further confirmed by MD simulation results that such small layer space is not conducive to the adsorption of a large number of cations (Zhang et al. 2022). Thus, high ionic strength reduces the adsorption amount by inhibiting the swelling of Mt.

510

511 **5.2 Competing cations**

512 Most previous studies have extensively examined the effects of solution pH, ionic
513 strength, and cation concentration on the adsorption extent of metal cations onto Mt,
514 whereas relatively little attention is paid to the ionic composition of the solution. Indeed,
515 common metal cations, such as Zn^{2+}, Mg^{2+}, Ca^{2+}, Na^{+} and K^{+} are ubiquitous in nature and
516 they tend to coexist in real-world clayey environments, such as soils and natural waters
517 (Orucoglu et al., 2022). In this regard, the competitive adsorption of metal cations may
518 occur either by cation exchange or surface complexation. Thus far, direct evidence for
519 such competitive adsorption phenomena has proven elusive, although the nature of
520 individual cations was successfully probed by simulations and spectroscopic data
521 (Orucoglu et al., 2022).

522 Metal cations occupying the same sorption sites on edge surfaces are among the
523 reasons for competitive adsorption phenomena. So far, gaining a mechanistic
524 understanding of competitive adsorption process of cations on Mt edge surfaces is
525 achieved mainly through mathematical modeling of adsorption data (Orucoglu et al.,
526 2022). For example, Sugiura et al. (2021) investigated the competitive adsorption
527 behavior of Ca^{2+}, Sr^{2+}, and Ni^{2+} cations on edge surfaces of Kunipia F Na-Mt under
528 alkaline conditions. Curve fitting analysis of the adsorption isotherms and edges obtained
529 at various $NaClO_4$ concentrations was carried out based on the 2SPNE SC/CE
530 thermodynamical model. The results indicated that Ca^{2+} and Sr^{2+} species were adsorbed
531 on the same edge sites ($\equiv S^{W2}OH$; site capacity = 40 mmol kg^{-1}) whereas Ni^{2+} was
532 preferred sorbed at the $\equiv S^{S}OH$ groups having a smaller site capacity of 2 mmol kg^{-1}.

Therefore, it is obvious that Ca^{2+} and Sr^{2+} ions compete with each other for weak adsorption sites at Mt edges (**Fig. 8A**), while the adsorption of Ni^{2+} on strong edge sites is not affected by the presence of Ca^{2+} cation (**Fig. 8B**). This work further showed that the single-metal sorption model parameters (i.e., K_{GT} and K_C) obtained from batch experiments can be applied to satisfactorily reproduce the competition effects in binary Ca–Sr and Ca–Ni systems. Studies have also suggested that adsorption of metal cations onto Mt is selective, that is, only metal cations with similar chemical attributes, such as valence state and hydrolysis behavior can potentially compete with each other (Bradbury and Baeyens, 2005a; Soltermann et al., 2014; Fernandes and Baeyens, 2019). Based on this consensus, Ca^{2+} competes strongly with other alkaline earth metal cations (e.g., Ba^{2+}, Ra^{2+}, Mg^{2+}) for the same edge adsorption sites but does not or minimally competes with transition (e.g., Mn^{2+}, Fe^{2+}, Fe^{3+}, Co^{2+}, and Ni^{2+}) and zinc group metals (Zn^{2+} and Cd^{2+}), which preferentially resided at the $\equiv S^{S}OH$ sites (Sugiura et al., 2021).

It is also implied from surface complexation modeling study that the competitive adsorption of metal cations on edge surfaces is not necessarily related to the binding site occupancy, but also due to the changes in local structure and/or electrostatic field as a result of co-ion adsorption onto different but adjacent sites (Orucoglu et al., 2022). Recently, the competitive adsorption of Pb^{2+}, Co^{2+}, and Mg^{2+} cations on edge surfaces was modeled with a state-of-art electrostatic complexation model incorporating spillover effect (Orucoglu et al., 2022). The modeling results indicated that the latter cation competes indirectly with Pb^{2+} and Co^{2+} (**Fig. 8D**) although the adsorption site of Mg^{2+} (S_a) is different with those of Pb^{2+} and Co^{2+} species (S_e sites). In this regard, the surface electrostatic potential of Mt edges becomes less negative upon adsorption of Mg^{2+} (**Fig.**

556 **8C**) and thus results in a decrease of the Pb^{2+} adsorption. It then follows that the
557 mechanism of competitive adsorption of cations on the Mt surface may depend to some
558 extent on the adsorption model used. Therefore, it is very important to improve the
559 understanding of surface properties of Mt itself and the combination of cations and Mt to
560 establish an accurate adsorption model.

561 Cation exchange dominates metal adsorption processes at low pH and ionic strength
562 conditions, due to the permanent structural negative charge. However, unlike adsorption
563 on edge surfaces, the cation uptake dynamics on basal face is weakly affected by the
564 presence of co-ions, suggesting that competitive adsorption does not change the
565 adsorption mechanisms of metal cations on Mt basal surface and only modify the
566 adsorption amounts and mobility of metal cations (Yang et al., 2018, 2020, 2021). Here,
567 the competitive behavior of cation exchange reactions is distinctly different from that of
568 edge surface adsorption since the driving forces between these two retention modes are
569 different. Alkali and alkaline earth cations rarely compete directly with heavy metals or
570 radioactive cations for adsorption on edge surface groups, thus, they are generally
571 regarded as competitors for cation exchange sites (Orucoglu et al., 2022). For example,
572 adsorption of heavy metals, such as Cu^{2+}, Pb^{2+} and Cr^{2+} was found to usually inhibited by
573 the presence of Ca^{2+} and Mg^{2+}, where the inhibition effect is greater for Ca^{2+} than that of
574 Mg^{2+} in accordance with stronger adsorption affinity of Mt for Ca^{2+} (Sposito et al., 1983;
575 Zhu et al., 2011). The Al^{3+} and Fe^{3+} cations also compete with heavy metals at low pH but
576 much stronger than Ca^{2+} and Mg^{2+}, owing to the higher charge density of the trivalent
577 cations. In general, competitive adsorption via cation exchange depends on the adsorption
578 affinity of Mt for cations that lead the adsorption selectivity. Although the valence state,

579 hydration and dispersion force of cations control the selectivity for adsorption on Mt,
580 these theoretical explanations have their limitations (Liu et al., 2013b).

581 Although most studies show that competitive adsorption leads to a decrease in the
582 amount of cations adsorbed by Mt, some studies have obtained the opposite results, that
583 is, increase in the adsorbed amount (Zhu et al., 2011; Ghorbel-Abid and Trabelsi-Ayadi,
584 2015; Yang et al., 2018). The amount of cations adsorbed on Mt surface may induce
585 promote/suppress effects, depending on the composition of metal cations in the solution,
586 pH and ionic strength (Zhu et al., 2011; Fernandes and Baeyens, 2019; Yang et al., 2018,
587 2021). For example, the existence of Pb^{2+} on Mt surface promotes Cs^{+} and Na^{+}
588 adsorption but inhibits Cd^{2+} adsorption (Yang et al., 2018). The Al^{3+} and Fe^{3+} compete
589 with Cu^{2+}, Pb^{2+} and Cr^{2+} at low pH, whereas Al^{3+} and Fe^{3+} at relatively high
590 concentrations could promote the adsorption of Cu^{2+}, Pb^{2+} and Cr^{2+} at relatively high pH
591 (**Fig. 9**) (Zhu et al., 2011). The possible reason that Al^{3+} and Fe^{3+} promote the adsorption
592 of heavy metal cations on Mt is that they will form polymers and nano-precipitates that
593 are irreversibly adsorbed on Mt surface under higher concentration and pH conditions,
594 thereby forming hydroxyl-Al or hydroxyl-Fe-intercalated Mt or amorphous-Al- or
595 amorphous-Fe-oxyhydroxide-coated Mt that has greater adsorption capacity than the
596 untreated Mt (Zhu et al., 2011; Franco et al., 2016; Almasri et al., 2018; Missana et al.,
597 2021;).

598 Compared to the simplified sorption systems studied in most laboratory experiments,
599 the presence of a large number of chemical species in the natural environments leads to
600 differences in the competitive adsorption of metal cations on Mt surfaces (Orucoglu et al.,
601 2022). A study on adsorption of Ra^{2+} on Na-Mt, ferrihydrite, goethite and pyrite under

similar ionic strength (10 mM), initial concentration of Ra^{2+} and pH (7.0) but with different background electrolytes showed that the adsorption of Ra^{2+} on Na-Mt was highest (**Fig. 10**) (Chen and Kocar, 2018). Also, the adsorption of Ra^{2+} under artificial groundwater (AGW) background electrolyte showed maximum decrease (**Fig. 10**). The antagonistic effect between the cations in water may have resulted in less Ra adsorption (Chen and Kocar, 2018). For example, CO_3^{2-} and Ca^{2+} commonly present in groundwater will form ternary calcium-uranyl carbonate complexes including $CaUO_2(CO_3)_2^{2-}{}_{(aq)}$ and $Ca_2UO_2(CO_3)_{3(aq)}$ with uranium, which are stable in solution and are not adsorbed on Mt surface (Tran et al., 2018). Obviously the adsorption of cations on Mt in the natural environment is different from the simplified systems in laboratory experiments.

5.3 Temperature

Compared with the solution properties, such as pH and ionic strength, there are still relatively few studies that address the effects of temperature on the interfacial properties of Mt surfaces and their adsorption behavior towards metal ions. In geological environments, Mt and other clay minerals are often prolongly exposed to a range of temperatures, from about 25-30 °C in natural soil systems (Angove et al., 1998), to 70-90 °C in the vicinity of the nuclear waste repositories (or even can reach 150 °C in some cases due to radioactive effects) (Bauer et al., 2005; Tertre et al., 2005, 2006; Zhang et al., 2018a), and to ~100 °C in medium-depth ocean basins (Liu et al., 2015). It is of importance to elucidate the role of temperature. While cation exchange reaction is essentially temperature independent (Tertre et al., 2005), such significant variations of temperatures would have an impact on the surface chemistry of Mt, such as structure,

acidity constants (pK_a), and the point of zero charge (PZC), thereby affecting surface complexation reactions of metal cations on edge surfaces (Liu et al., 2015).

With regard to temperature, adsorption process can be classified as either physical or chemical. The influence of temperature on the cation adsorption onto Mt and the associated energetic changes can be described in terms of thermodynamic parameters, such as the changes in enthalpy (ΔH), entropy (ΔS), and Gibbs free energy (ΔG), whose values for several Mt–cation systems are listed in **Table 3**. It can be seen that metal adsorption processes at Mt surfaces are spontaneous ($\Delta G < 0$), regardless of temperature, and this environmental factor positively affects the uptake of most transition metal ions, such as Ni^{2+}, Mn^{2+}, Fe^{3+}, Cr^{3+}, and so forth (Tertre et al., 2005, 2006; Tan et al., 2011; Yu et al., 2016). For example, the adsorption of Ni^{2+} on Mt is found to be endothermic ($\Delta H > 0$), in which the adsorption capacity increases with increasing temperature (Tahir and Rauf, 2003; Yu et al., 2016). In addition to enhancing the adsorption capacity, increasing temperature may promote the migration of Ni^{2+} cations from weak to strong binding sites, that is, less sterically accessible sites or the transition of adsorption modes from outer- to inner-sphere (Tan et al., 2011; Yu et al., 2016). It is also demonstrated that the energy required for dehydration of fully-solvated cations is greater than that released during the outer- to inner-sphere complex transition (Hu et al., 2012), thus higher temperatures benefit the. Similar observations were reported for the sorption behavior of Mn^{2+} and Eu^{3+} ions on Mt. Meanwhile, the ΔH values of some metal cations, such as Cs^{+} and Pb^{2+} are negative, indicating the exothermicity of adsorption process on Mt. In these cases, an increase in temperature reduces the adsorption amount of Pb^{2+} on Mt (Gupt, et al. 2020), and MD simulations indicate that temperature controls the adsorption process of Pb^{2+} by

changing the maximum adsorption energy of Mt and the diffusion and hydration state of Pb^{2+} (Du et al., 202). Specifically, the diffusion coefficient and the first peak value of radial distribution function curve of Pb^{2+} to water oxygen (H_1) both increase with temperature (**Fig. 11A and B**). Under this concentration range of 0.1-0.5 M, the adsorbed Pb^{2+} cations on Mt edges remain predominantly as an OSSC. When the adsorbed amount reaches saturation, the adsorption energy decreases at higher temperature, thus leading to the diminishing uptake capacity (**Fig. 11C**). It is also important to mention that the chemical and structural alterations of Mt affect the thermodynamic sorption parameters. For example, the ΔH parameter for Ni^{2+} adsorption on calcined Mt showed a negative value, whereas this value is positive for retention of the same cation on natural Mt.

MD simulation results have shown that the elevated temperature can only accelerate the cation exchange reaction while not changing the amount (**Fig. 11D**), and it is speculated that the increase of adsorption amount is derived from the cations adsorbed at Mt edge surface rather than basal surface (Zhang et al. 2022). This viewpoint is further confirmed by the first principles molecular dynamics (FPMD) simulations of Mt edge sites, showing that the $\equiv Al(OH_2)_2$, $\equiv Al(OH_2)$ sites on [010] surface, and $Al(OH_2)$ sites on [110] surface are the main adsorption sites on Mt edge surface in the temperature range from 298 to 423 K (Liu et al., 2015; Zhang et al., 2018a). The stability of the $\equiv Al(OH_2)$ on [010] edge surface increases with temperature, suggesting that $\equiv Al(OH_2)$ sites bind metal cations more easily at higher temperatures (Liu et al., 2015). Moreover, acid-base titration experiments and FPMD simulations have shown that the pK_a value of Mt edge surface decreased with temperature, suggesting that the number of complexation

sites increases with temperature at the same pH (Duc et al., 2008; Rozalen et al., 2009; Liu et al., 2015).

5.4 Charge density and localization

The negative lattice charge of Mt arising from isomorphic cation substitutions plays a key role in their high sorption capacity of this clay mineral for cations (Li et al., 2012b, 2019a, 2021a, 2021b). Similar other naturally occurring materials, Mt of different origins may have different chemical compositions, which might affect the density and localization of the layer charge (Hetzel and Doner, 1993). As cation adsorption onto the basal surface of Mt is governed by electrostatic forces, Mt with higher layer charge densities and/or layer charge closely located near the O-Si-O tetrahedral sheets are more favorable for cation adsorption (Liu et al., 2008; Yang et al., 2020; Liu et al., 2021). The relationships between the adsorbed cations on the basal surface and the charge density and distribution of Mt are summarized in **Table 4**.

The increase of the layer charge density of Mt, particularly tetrahedral charge, promotes the inner-sphere adsorption of cations and enhances the potential energy (or stability) of the resultant complexes **(Table 4)** (Yang et al., 2020; Li et al., 2021b). For example, MD simulation results indicated that the distance of adsorbed Pb^{2+} and Ba^{2+} ions to Mt basal surface were decreased with increasing charge density and part of them were closer than one monolayer of H_2O, which indicated that the adsorption mode of Pb^{2+} and Ba^{2+} changed from outer-sphere to inner-sphere (**Fig. 12A**) (Zhang et al., 2023). In addition, heavy metal cations, such as Zn^{2+}, Cd^{2+}, and Pb^{2+} form outer-sphere complexes upon adsorption to the basal surface of Mt with octahedral charge only (Gu et al., 2010;

693 Liu et al., 2021), while Cd^{2+} and Pb^{2+} formed inner-sphere species on Mt with both
694 octahedral and tetrahedral charge sites (**Fig. 12B**) (Liu et al., 2021). Thus, adsorbed
695 cations form more easily inner-sphere complexes on Mt with tetrahedral charge, mainly
696 due to the stronger attractive electrostatic interactions between the tetrahedral charge sites
697 and metal cations compared to Mt with octahedral charge (Liu et al., 2021). However, the
698 adsorption modes of Cs^{+} and Zn^{2+} do not seem to change no matter the charge density or
699 charge location (Fig.12A and B). This is thought to be related to differences in hydration
700 energy of cations. The much higher absolute value of hydration energy of Zn^{2+}
701 (experimentally measured as − 467 kcal/mol) leads to the more firmly combination
702 between Zn^{2+} and water molecules, and lower absolute value of hydration energy of Cs^{+}
703 (experimentally measured as − 277 kcal/mol) results in that it is not easy to be completely
704 combined with water molecules and is easily adsorbed by negatively charged Mt layers
705 (Liu et al., 2021; Zhang et al., 2023).

706 Apart from the inner-sphere and outer-sphere complexation of metal cations, the
707 charge location also profoundly affects their distribution on Mt basal surface. For
708 example, the adsorption sites of Na^{+} ions occur near isomorphic substitutions where the
709 negative charge is more concentrated (Chatterjee et al., 1999). The time-evolution
710 trajectories showed that Zn^{2+}, Cd^{2+}, and Pb^{2+} ions tend to reside close to the tetrahedral Al
711 of Wyoming Mt, which has both octahedral and tetrahedral charge sites, while random
712 distributions were observed on the Arizona Mt with only octahedral charge sites (**Fig.**
713 **12C**). This indicates that the mobility of cations on Wyoming Mt basal surface is lower
714 than on Arizona Mt basal surface due to the presence of tetrahedral charge sites (Yang et
715 al., 2019; Liu et al., 2021). Although the density and localization of the Mt layer charge

716 seem to control the amount of adsorbed cations and adsorption sites for most cations,
717 some cations, such as K^+, Cs^+, and Zn^{2+} were almost unaffected by the layer charge
718 density and localization (Babu and Lim, 2006; Churakov, 2013; Li et al., 2019b; Yang et
719 al., 2019; Rahromostaqim and Sahimi, 2020; Yang et al., 2020; Liu et al., 2021). The
720 hydration interactions of these three ions may be the reason for this exception.

721 The electrostatic potential of the edge surfaces (Ψ) is a critical parameter in SCMs for
722 predicting the adsorption behavior of cations onto Mt edge surfaces. In most previous
723 studies, Ψ is usually determined by the classical Gouy-Chapman model based on the
724 Poisson-Boltzmann equation (PBE) or by assuming that Ψ is equal to zero (Bradbury and
725 Baeyens, 1997; Montavon et al., 2006; Gu et al., 2010). However, studies exploring the
726 relationship between the charge density and edge surface potential of clay minerals
727 suggest that Ψ is different from that predicted by the Gouy-Chapman model (Secor and
728 Radke, 1985; Chang and Sposito, 1994, 1996; Kraepiel et al., 1998). Moreover, the value
729 of Ψ is affected by the charge density of the edge and basal surface and is sensitive to the
730 arrangement of Mt layers and solution ionic strength (**Fig. 13A and B**) (Kraepiel et al.,
731 1998; Bourg et al., 2007; Tournassat et al., 2013). The effect of the basal surface charge
732 on the edge surface potential is called the spillover effect (Pecini and Avena, 2013). The
733 spillover effect influences the charge-electrostatic potential relationship, thus changing
734 the contribution of the adsorption force and affecting the adsorption of metal cations on
735 Mt edge surface. The relationship between Ψ and edge charge density (Q) can be
736 expressed by the following formula:

737 $$\frac{F\Psi}{RT} = A_1 \mathrm{asinh}[A_2(Q_{edge} + A_3)] \quad (8)$$

where A_1, A_2 and A_3 are parameters fitted with the Ψ values and are related to ionic strengths. Compared with the traditional SCM, the modified SCM incorporating the spillover effect predicts the adsorption of metal cations on Mt edge surface more accurately (Tournassat et al., 2018; Orucoglu et al., 2022).

6. Implications

In natural environments, Mt is involved in a complex variety of surface reactions that control the fates of metal cations including their chemical speciation, transformation, and bioavailability. Sorption of metal cations by Mt mainly occurs by cation exchange and surface complexation reactions. Surface precipitation is another means of sequestering metal cations that generally takes place at high concentration and pH conditions (i.e., alkaline soils). In these adsorption processes, metal cations interact with Mt surfaces by electrostatic force, covalent bond, hydrogen bonding and van der Waals force. In addition to the characteristics of Mt, environmental conditions, such as ionic strength, pH, competing cations, background electrolyte, and temperature have profound influences on the adsorption amount and affinity of metal cations for Mt surfaces. Thus, an in-depth understanding of the adsorption characteristics and interfacial interactions between metal cations and the Mt surfaces could drive for practical applications in geological engineering, environmental remediation, and industrial processes.

As a critical component of solid soil matrices, Mt can adsorb and retain a large number of metal pollutants that are harmful to humans, reducing their bioavailability and thus the potential toxicity at contaminated sites. The strong interfacial interactions between metal cations and Mt surfaces through formation of complexes are crucial for

761 preventing the release of metal cations into the environment, which contributes to
762 efficient remediation of heavy metals and restoration of soil quality. Moreover, the
763 presence of Mt in soils represents an important reservoir for maintaining supply of
764 common biological cations, such as K^+, Na^+, Ca^{2+}, and Mg^{2+} to promote sustainable
765 agricultural production. In addition to agricultural practices, the interaction of these soil
766 nutrient cations with interlayer surfaces of Mt plays an important role in the diagenesis of
767 clay minerals, such as illitization. During this transformation process, exchange of
768 interlayer Na^+/Ca^{2+} in Mt with K^+ ions is thought to be the rate-controlling step, hence a
769 quantitative and molecular understanding of these interfacial interactions under relevant
770 geological conditions is essential to predict the extent and rate of illitization. Such
771 insights on the cation–Mt interactions during mineralization also have implications for
772 the formation of oil and metal ores, paleoclimate evolution, and stratigraphic division.

773 In the context of aquatic environments, Mt is widely regarded as a low-cost and
774 environmentally friendly adsorbent material for the remediation of water and wastewater
775 containing toxic metals. Various heavy metals and radionuclides can be effectively
776 removed by Mt from aqueous environmental systems and industrial wastewater which the
777 composition is very complex. The interfacial interactions between metal cations and Mt
778 under different pH values, temperatures, and presence of carbonates and organic matter
779 compounds are crucial for the improvement of Mt surface modification strategies and the
780 development of Mt-based adsorbents that are suitable for much types of industrial
781 wastewater. Besides, the immobilization of metal cations on Mt has been of great interest
782 for chemical industry since it offers an attractive means for producing low-cost
783 heterogeneous catalysts, where Mt can act as the support matrix or directly as solid acid.

While the microenvironment of the adsorbed catalytically active metal cations may change due to the interfacial charge transfer, structure change, or molecular adsorption modulation, due to the layer charge and active surface groups of Mt. Further study on the interfacial interactions between metal cations and Mt are conducive for the development of metal-based Mt catalysts with high activity, selectivity, and stability for performing various industrially important reactions. Furthermore, the dispersion, swelling, expansion and suspension properties of Mt in water and organic solvents are closely related to the interactions of metal cations, water molecules and Mt surfaces, which may promote the applications of Mt as a common rheological agent in cosmetics, paint, medicine, and oil exploitation.

Conflicts of interest

There are no conflicts to declare.

Acknowledgements

The authors wish to acknowledge the financial support from the National Natural Science Foundation of China (22072136；41672033)，the research grants from Engineering Research Center of Non-metallic Minerals of Zhejiang Province (ZD2020K07)，and the projects from Qing Yang Institute for Industrial Minerals (KYY-HX-20220336;KYY-HX-20170557).

References

Akpomie, K.G., Dawodu, F.A., and Adebowale, K.O. (2015) Mechanism on the sorption of heavy metals from binary-solution by a low cost montmorillonite and its desorption potential. Alexandria Engineering Journal, 54(3), 757-767.

Almasri, D.A., Rhadfi, T., Atieh, M.A., McKay, G., and Ahzi, S. (2018) High performance hydroxyiron modified montmorillonite nanoclay adsorbent for arsenite removal. Chemical Engineering Journal, 335, 1-12.

Anderson, R.L., Ratcliffe, I., Greenwell, H.C., Williams, P.A., Cliffe, S., and Coveney, P.V. (2010) Clay swelling — A challenge in the oilfield. Earth-Science Reviews, 98(3-4), 201-216.

Angove, M.J., Johnson, B.B., and Wells, J.D. (1998) The influence of temperature on the adsorption of cadmium(II) and cobalt(II) on kaolinite. Journal of Colloid and Interface Science, 204, 93-103.

Babu, C.S., and Lim, C. (2006) Empirical force fields for biologically active divalent metal cations in water. Journal of Physical Chemistry A, 110(2), 691-699.

Baeyens B, and Bradbury M. H. (2002) Sorption of Eu on Na- and Ca- montmorillonites: experimental investigations and modelling with cation exchange and surface. Geochimica et Cosmochimica Acta, 66(13), 2325-2334.

Balali-Mood, M., Naseri, K., Tahergorabi, Z., Khazdair, M.R., and Sadeghi, M. (2021) Toxic mechanisms of five heavy metals: Mercury, lead, chromium, cadmium, and arsenic. Front Pharmacol, 12, 643972.

826 Balasubramanian, R., Perumal, S.V., and Vijayaraghavan, K. (2009) Equilibrium isotherm
827 studies for the multicomponent adsorption of lead, zinc, and cadmium onto
828 indonesian peat. Industrial & Engineering Chemistry Research, 48(4), 2093-2099.
829 Bauer, A., Rabung, T., Claret, F., Schäfer, T., Buckau, G., and Fanghänel, T. (2005)
830 Influence of temperature on sorption of europium onto smectite: The role of
831 organic contaminants. Applied Clay Science, 30(1), 1-10.
832 Bhattacharyya, K. (2008) Kaolinite and montmorillonite as adsorbents for Fe(III), Co(II)
833 and Ni(II) in aqueous medium. Applied Clay Science, 41(1-2), 1-9.
834 Bhattacharyya, K.G., and Gupta, S.S. (2007) Adsorptive accumulation of Cd(II), Co(II),
835 Cu(II), Pb(II), and Ni(II) from water on montmorillonite: influence of acid
836 activation. Journal of Colloid and Interface Science, 310(2), 411-424.
837 Bickmore, B.R., Rosso, K.M., Nagy, K.L., Cygan, R.T., and Tadanier, C.J. (2003) Ab
838 initio determination of edge surface structures for dioctahedral 2:1
839 phyllosilicates:Implications for acid-base for reactivity. Clays and Clay Minerals,
840 51(4), 359-371.
841 Borisover, M., and Davis, J.A. (2015) Adsorption of inorganic and organic solutes by clay
842 minerals. Natural and Engineered Clay Barriers, p. 33-70.
843 Bourg, I.C., and Sposito, G. (2011) Molecular dynamics simulations of the electrical
844 double layer on smectite surfaces contacting concentrated mixed electrolyte
845 ($NaCl$-$CaCl_2$) solutions. Journal of Colloid and Interface Science, 360(2),
846 701-715.

847 Bourg, I.C., Sposito, G., and Bourg, A.C.M. (2007) Modeling the acid-base surface
848 chemistry of montmorillonite. Journal of Colloid and Interface Science, 312(2),
849 297-310.
850 Bradbury, M.H., and Baeyens, B. (1997) A mechanistic description of Ni and Zn sorption
851 on Na-montmorillonite Part II: Modelling. Journal of Contaminant Hydrology, 27,
852 223-248.
853 Bradbury, M.H., and Baeyens, B. (2002) Sorption of Eu on Na- and Ca-montmorillonites:
854 Experimental investigations and modelling with cation exchange and surface
855 complexation. Geochimica et Cosmochimica Acta, 66(13), 2325–2334.
856 Bradbury, M.H., and Baeyens, B. (2005a) Experimental measurements and modeling of
857 sorption competition on montmorillonite. Geochimica et Cosmochimica Acta,
858 69(17), 4187-4197.
859 Bradbury, M.H., and Baeyens, B. (2005b) Modelling the sorption of Mn(II), Co(II),
860 Ni(II), Zn(II), Cd(II), Eu(III), Am(III), Sn(IV), Th(IV), Np(V) and U(VI) on
861 montmorillonite: Linear free energy relationships and estimates of surface binding
862 constants for some selected heavy metals and actinides. Geochimica et
863 Cosmochimica Acta, 69(4), 875-892.
864 Chang, F.R.C., and Sposito, G. (1994) The electrical double layer of a disked-shaped clay
865 mineral particle: Effect of particle size. Journal of Colloid and Interface Science,
866 163, 19-27.
867 Chang, F.R.C., and Sposito, G. (1996) The electrical double layer of a disked-shaped clay
868 mineral particle: Effect of electrolyte properties and surface charge density.
869 Journal of Colloid and Interface Science, 178, 555−564.

Chatterjee, A., Iwasaki, T., Ebina, T., and Miyamoto, A. (1999) A DFT study on clay-cation-water interaction in montmorillonite and beidellite. Computational Materials Science, 14, 119-124.

Chen, M.A., and Kocar, B.D. (2018) Radium sorption to iron (hydr)oxides, pyrite, and montmorillonite: Implications for mobility. Environmental Science & Technology, 52(7), 4023-4030.

Cherif, M.A., Martin-Garin, A., Gerard, F., and Bildstein, O. (2017) A robust and parsimonious model for caesium sorption on clay minerals and natural clay materials. Applied Geochemistry, 87, 22-37.

Churakov, S.V. (2013) Mobility of Na and Cs on montmorillonite surface under partially saturated conditions. Environmental Science & Technology, 47(17), 9816-9823.

Churakov, S.V., and Dähn, R. (2012) Zinc adsorption on clays inferred from atomistic simulations and EXAFS spectroscopy. Environmental Science & Technology, 46(11), 5713-5719.

Cygan, R.T., Liang, J.J., and Kalinichev, A.G. (2004) Molecular models of hydroxide, oxyhydroxide, and clay phases and the development of a general force field. Journal of Physical Chemistry B, 108(4), 1255-1266.

Dähn, R., Baeyens, B., and Bradbury, M.H. (2011) Investigation of the different binding edge sites for Zn on montmorillonite using P-EXAFS – The strong/weak site concept in the 2SPNE SC/CE sorption model. Geochimica et Cosmochimica Acta, 75(18), 5154-5168.

Dähn, R., Scheidegger, A.M., Manceau, A., Schlegel, M.L., Baeyens, B., Bradbury, M.H., and Chateigner, D. (2003) Structural evidence for the sorption of Ni(II) atoms on

the edges of montmorillonite clay minerals: A polarized X-ray absorption fine structure study. Geochimica et Cosmochimica Acta, 67, 1-15.

de Pablo, L., Chávez, M.L., and Abatal, M. (2011) Adsorption of heavy metals in acid to alkaline environments by montmorillonite and Ca-montmorillonite. Chemical Engineering Journal, 171(3), 1276-1286.

Du, J.P., Zhou, A.N., Lin, X.S., and Bu, Y.H. (2022) Adsorption mechanism of Pb^{2+} in montmorillonite nanopore under various temperatures and concentrations. Environmental Research, 209, 112817.

Duc, M., Carteret, C., Thomas, F., and Gaboriaud, F. (2008) Temperature effect on the acid–base behaviour of Na-montmorillonite. Journal of Colloid and Interface Science, 327(2), 472-476.

Duran, J.D., Ramos-Tejada, M.M., Arroyo, F.J., and Gonzalez-Caballero, F. (2000) Rheological and electrokinetic properties of sodium montmorillonite suspensions. Journal of Colloid and Interface Science, 229(1), 107-117.

Fernandes, M.M., and Baeyens, B. (2019) Cation exchange and surface complexation of lead on montmorillonite and illite including competitive adsorption effects. Applied Geochemistry, 100, 190-202.

Ferrage, E., Lanson, B., Michot, L.J., and Robert, J.-L. (2010) Hydration properties and interlayer organization of water and ions in synthetic Na-smectite with tetrahedral layer charge. Part 1. Results from X-ray diffraction profile modeling. Journal of Physical Chemistry C, 114, 4515-4526.

Ford, R.G., and Sparks, D.L. (2000) The nature of Zn precipitates formed in the presence of pyrophyllite. Environmental Science & Technology, 34, 2479–2483.

916 Franco, F., Benitez-Guerrero, M., Gonzalez-Trivino, I., Perez-Recuerda, R., Assiego, C.,
917 Cifuentes-Melchor, J., and Pascual-Cosp, J. (2016) Low-cost aluminum and iron
918 oxides supported on dioctahedral and trioctahedral smectites: A comparative study
919 of the effectiveness on the heavy metal adsorption from water. Applied Clay
920 Science, 119, 321-332.
921 Fukushi, K., Sakai, H., Itono, T., Tamura, A., and Arai, S. (2014) Desorption of intrinsic
922 cesium from smectite: Inhibitive effects of clay particle organization on cesium
923 desorption. Environmental Science & Technology, 48(18), 10743-10749.
924 Gaines, G.L.J., and Thomas, H.C. (1953) Adsorption studies on clay minerals. II. A
925 formulation of the thermodynamics of exchange adsorption. Journal of Chemical
926 Physics, 21, 714-718.
927 Gao, P.Y., Zhang, D.M., Jin, Q., Chen, Z.Y., Wang, D.Q., Guo, Z.J., and Wu, W.S. (2021)
928 Multi-scale study of Am(III) adsorption on Gaomiaozi bentonite: Combining
929 experiments, modeling and DFT calculations. Chemical Geology, 581, 120414.
930 Gao, P., Liu, X., Guo, Z., Tournassat, C. (2023) Acid–base properties of cis-vacant
931 montmorillonite edge surfaces: A combined first-principles molecular dynamics
932 and surface complexation modeling approach. Environmental Science &
933 Technology, 57, 1342-1352.
934 Ghasemi, M., and Sharifi, M. (2021) Effects of layer-charge distribution on swelling
935 behavior of mixed-layer illite-montmorillonite clays: A molecular dynamics
936 simulation study. Journal of Molecular Liquids, 335, 116188.
937 Ghorbel-Abid, I., and Trabelsi-Ayadi, M. (2015) Competitive adsorption of heavy metals
938 on local landfill clay. Arabian Journal of Chemistry, 8(1), 25-31.

939 Gu, X.Y., Evans, L.J., and Barabash, S.J. (2010) Modeling the adsorption of Cd (II), Cu
940 (II), Ni (II), Pb (II) and Zn (II) onto montmorillonite. Geochimica et
941 Cosmochimica Acta, 74(20), 5718-5728.
942 Guggenheim, S., Adams, J.M., Bain, D.C., Bergaya, F., Brigatti, M.F., Drits, V.A.,
943 Formoso, M.L.L., Galan, E., Kogure, T., and Stanjek, H. (2006) Summary of
944 recommendations of nomenclature committees relevant to clay mineralogy: report
945 of the Association Internationale pour l'Etude des Argiles (AIPEA) Nomenclature
946 Committee for 2006. Clay Minerals, 41(4), 863-877.
947 Gupt, C.B., Bordoloi, S., Sekharan, S., and Sarmah, A.K. (2020) Adsorption
948 characteristics of Barmer bentonite for hazardous waste containment application.
949 Journal of Hazardous Materials, 396, 122594.
950 Halim, M., Conte, P., and Piccolo, A. (2003) Potential availability of heavy metals to
951 phytoextraction from contaminated soils induced by exogenous humic substances.
952 Chemosphere, 52(1), 265-275.
953 Hennig, C., Reich, T., Dähn, R., and Scheidegger, A.M. (2002) Structure of uranium
954 sorption complexes at montmorillonite edge sites. Radiochim. Acta, 90, 653-657.
955 Hetzel, F., and Doner, H.E. (1993) Some colloidal properties of beidellite-comparision
956 with Low and high charge montmorillonites. Clays and Clay Minerals, 41,
957 453-460.
958 Hrobáriková, J., Madejová, J., and Komadel, P. (2001) Effect of heating temperature on
959 Li-fixation, layer charge and properties of fine fractions of bentonites. Journal of
960 Materials Chemistry, 11(5), 1452-1457.

961 Hu, J., Tan, X., Ren, X., and Wang, X. (2012) Effect of humic acid on nickel(II) sorption
962 to Ca-montmorillonite by batch and EXAFS techniques study. Dalton Trans,
963 41(35), 10803.
964 Huang, W.J., Liu, J.H., She, Q.M., Zhong, J.Q., Christidis, G.E., and Zhou, C.H. (2021)
965 Recent advances in engineering montmorillonite into catalysts and related
966 catalysis. Catalysis Reviews, 1-57.
967 Jenny, H. (1931) Studies on the mechanism of ionic exchange in colloidal aluminum
968 silicates. Journal of Physical Chemistry C, 36, 2217-2258.
969 Jenny, H. (1935) Simple kinetic theory of ionic exchange. I Ions of equal valency. Journal
970 of Physical Chemistry C, 40, 501-517.
971 Kim, Y., Cygan, R.T., and Kirkpatrick, R.J. (1996) ^{133}Cs NMR and XPS investigation of
972 cesium adsorbed on clay minerals and related phases. Geochimica et
973 Cosmochimica Acta, 60, 1041-1052.
974 Kraepiel, A.M.L., Keller, K., and Morel, F.M.M. (1998) On the acid-base chemistry of
975 permanently charged minerals. Environmental Science & Technology, 32(19),
976 2829-2838.
977 Kraevsky, S.V., Tournassat, C., Vayer, M., Warmont, F., Grangeon, S., Wakou, B.F.N.,
978 and Kalinichev, A.G. (2020) Identification of montmorillonite particle edge
979 orientations by atomic-force microscopy. Applied Clay Science, 105442.
980 Kremleva, A., Kruger, S., and Rosch, N. (2015) Uranyl adsorption at solvated edge
981 surfaces of 2 : 1 smectites. A density functional study. Physical Chemistry
982 Chemical Physics, 17(20), 13757.

983 Kwon, K.D., and Newton, A.G. (2016) Structure and stability of pyrophyllite edge
984 surfaces: Effect of temperature and water chemical potential. Geochimica et
985 Cosmochimica Acta, 190, 100-114.
986 Lepore, G.O., Schingaro, E., Mesto, E., Lacalamita, M., Cristiani, C., Stampino, P.G.,
987 Dotelli, G., Finocchio, E., d'Acapito, F., and Giuli, G. (2022) Lanthanum captured
988 in montmorillonite: Evidence of inner-sphere complexes from X-ray absorption
989 spectroscopy investigations. Applied Clay Science, 230, 106676.
990 Li, Q.Y., Li, R., and Shi, W.Y. (2021a) Cation adsorption at permanently (montmorillonite)
991 and variably (quartz) charged mineral surfaces: Mechanisms and forces from
992 subatomic scale. Applied Clay Science, 213, 106245.
993 Li, Q.Y., Shi, W.Y., and Yang, Q.Y. (2021b) Polarization induced covalent bonding: A
994 new force of heavy metal adsorption on charged particle surface. Journal of
995 Hazardous Materials, 412, 125168.
996 Li, Q.Y., Yang, S., Tang, Y., Yang, G., and Li, H. (2019a) Asymmetric hybridization
997 orbitals at the charged interface initiates new surface reactions: A quantum
998 mechanics exploration. Journal of Physical Chemistry C, 123(41), 25278-25285.
999 Li, X., Liu, N., and Zhang, J. (2019) Adsorption of cesium at the external surface of TOT
1000 type clay mineral: Effect of the interlayer cation and the hydrated state. Journal of
1001 Physical Chemistry C, 123(32), 19540-19548.
1002 Li, X., Zhu, C., Jia, Z.Q., and Yang, G. (2018) Confinement effects and mechanistic
1003 aspects for montmorillonite nanopores. Journal of Colloid and Interface Science,
1004 523, 18-26.

Li, Y., Chen, M., Liu, C.J., Song, H.Z., Yuan, P., Zhang, B.F., Liu, D., and Du, P.X. (2020) Effects of layer-charge distribution of 2:1 clay minerals on methane hydrate formation: A molecular dynamics simulation study. Langmuir, 36(13), 3323-3335.

Li, Y.T., Narayanan Nair, A.K., Kadoura, A., Yang, Y.F., and Sun, S.Y. (2019b) Molecular simulation study of montmorillonite in contact with water. Industrial & Engineering Chemistry Research, 58(3), 1396-1403.

Liu, D., Du, W., Liu, X.M., Tian, R., and Li, H. (2019) To distinguish electrostatic, coordination bond, nonclassical polarization, and dispersion forces on cation–clay interactions. The Journal of Physical Chemistry C, 123(4), 2157-2164.

Liu, L.B., Zhang, C., Jiang, W.J., Li, X., Dai, Y.C., and Jia, H.Z. (2021) Understanding the sorption behaviors of heavy metal ions in the interlayer and nanopore of montmorillonite: A molecular dynamics study. Journal of Hazardous Materials, 416, 125976.

Liu, T., Tian, X.F., Zhao, Y., and Gao, T. (2010) Swelling of K^{+}, Na^{+} and Ca^{2+}-montmorillonites and hydration of interlayer cations: a molecular dynamics simulation. Chinese Physics B, 19, 109101.

Liu, X.D., Cheng, J., Sprik, M., Lu, X.C., and Wang, R.C. (2014a) Surface acidity of 2:1-type dioctahedral clay minerals from first principles molecular dynamics simulations. Geochimica et Cosmochimica Acta, 140, 410-417.

Liu, X.D., and Lu, X.C. (2006) A thermodynamic understanding of clay-swelling inhibition by potassium ions. Angewandte Chemie International Edition in English, 45(38), 6300-6303.

1027 Liu, X.D., Lu, X.C., Cheng, J., Sprik, M., and Wang, R.C. (2015) Temperature
1028 dependence of interfacial structures and acidity of clay edge surfaces. Geochimica
1029 et Cosmochimica Acta, 160, 91-99.
1030 Liu, X.D., Lu, X.C., Sprik, M., Cheng, J., Meijer, E.J., and Wang, R.C. (2013a) Acidity of
1031 edge surface sites of montmorillonite and kaolinite. Geochimica et Cosmochimica
1032 Acta, 117, 180-190.
1033 Liu, X.D., Lu, X.C., Wang, R.C., and Zhou, H.Q. (2008) Effects of layer-charge
1034 distribution on the thermodynamic and microscopic properties of Cs-smectite.
1035 Geochimica et Cosmochimica Acta, 72(7), 1837-1847.
1036 Liu, X.D., Meijer, E.J., Lu, X.C., and Wang, R.C. (2012a) First-principles molecular
1037 dynamics insight into Fe^{2+} complexes adsorbed on edge surfaces of clay minerals.
1038 Clays and Clay Minerals, 60(4), 341-347.
1039 Liu, X.D., Tournassat, C., Grangeon, S., Kalinichev, A.G., Takahashi, Y., and Fernandes,
1040 M.M. (2022) Molecular-level understanding of metal ion retention in clay-rich
1041 materials. Nature Reviews Earth & Environment, 3(7), 461-476.
1042 Liu, X.M., Li, H., Du, W., Tian, R., Li, R., and Jiang, X.J. (2013b) Hofmeister effects on
1043 cation exchange equilibrium: Quantification of ion exchange selectivity. The
1044 Journal of Physical Chemistry C, 117(12), 6245-6251.
1045 Liu, X.M., Li, H., Li, R., Tian, R., and Hou, J. (2012b) A new model for cation exchange
1046 equilibrium considering the electrostatic field of charged particles. Journal of
1047 Soils and Sediments, 12(7), 1019-1029.

1048 Liu, X.M., Li, H., Li, R., Xie, D.T., Ni, J.P., and Wu, L.S. (2014b) Strong non-classical
1049 induction forces in ion-surface interactions: General origin of Hofmeister effects.
1050 Scientific Reports, 4, 5047.
1051 Maes, A., and Cremers, A. (1977a) Charge density effects in ion exchange. Part
1052 1.—Heterovalent exchange equilibria. Journal of the Chemical Society, Faraday
1053 Transactions, 73, 1807-1814.
1054 Maes, A., and Cremers, A. (1977b) Charge density effects in ion exchange. Part
1055 2.—Homovalent exchange equilibria. Journal of the Royal Chemical Society,
1056 Faraday Transactions, 74, 1234-1241.
1057 Manning, B.A., and Goldberg, S. (1997) Adsorption and stability of arsenic(III) at the
1058 clay mineral-water interface. Environmental Science & Technology, 31,
1059 2005−2011.
1060 Marques Fernandes, M., Baeyens, B., Dähn, R., Scheinost, A.C., and Bradbury, M.H.
1061 (2012) U(VI) sorption on montmorillonite in the absence and presence of
1062 carbonate: A macroscopic and microscopic study. Geochimica et Cosmochimica
1063 Acta, 93, 262-277.
1064 Marques Fernandes, M., Scheinost, A.C., and Baeyens, B. (2016) Sorption of trivalent
1065 lanthanides and actinides onto montmorillonite: Macroscopic, thermodynamic and
1066 structural evidence for ternary hydroxo and carbonato surface complexes on
1067 multiple sorption sites. Water Research, 99, 74-82.
1068 Missana, T., Alonso, U., and Garcia-Gutierrez, M. (2021) Evaluation of component
1069 additive modelling approach for europium adsorption on 2:1 clays: Experimental,
1070 thermodynamic databases, and models. Chemosphere, 272, 129877.

1071 Montavon, G., Alhajji, E., and Grambow, B. (2006) Study of the interaction of Ni^{2+} and
1072 Cs^{+} on MX-80 bentonite: Effect of compaction using the “capillary method".
1073 Environmental Science & Technology, 40, 4672−4679.
1074 Newton, A., Kwon, K., and Cheong, D.K. (2016) Edge structure of montmorillonite from
1075 atomistic simulations. Minerals, 6(2), 25.
1076 Newton, A.G., and Sposito, G. (2015) Molecular dynamics simulations of pyrophyllite
1077 edge surfaces: Structure, surface energies, and solvent accessibility. Clays and
1078 Clay Minerals, 63(3-4), 277-289.
1079 Novikau, R., and Lujaniene, G. (2022) Adsorption behaviour of pollutants: Heavy metals,
1080 radionuclides, organic pollutants, on clays and their minerals (raw, modified and
1081 treated): A review. Journal of Environmental Management, 309, 114685.
1082 Ohkubo, T., Okamoto, T., Kawamura, K., Guegan, R., Deguchi, K., Ohki, S., Shimizu, T.,
1083 Tachi, Y., and Iwadate, Y. (2018) New insights into the Cs adsorption on
1084 montmorillonite clay from ^{133}Cs solid-state NMR and density functional theory
1085 calculations. The Journal of Physical Chemistry A, 122(48), 9326-9337.
1086 Orucoglu, E., Grangeon, S., Gloter, A., Robinet, J.-C., Madé, B., and Tournassat, C.
1087 (2022) Competitive adsorption processes at clay mineral surfaces: A coupled
1088 experimental and modeling approach. ACS Earth and Space Chemistry, 6(1),
1089 144-159.
1090 Ozdemir, G., and Yapar, S. (2009) Adsorption and desorption behavior of copper ions on
1091 Na-montmorillonite: effect of rhamnolipids and pH. Journal of Hazardous
1092 Materials, 166(2-3), 1307-1313.

1093 Ozsoy, O., and Bekbolet, M. (2018) Surface interactions of Cs^{+} and Co^{2+} with bentonite.
1094 Environmental Science and Pollution Research, 25(4), 3020-3029.
1095 Payne, T.E., Brendler, V., Ochs, M., Baeyens, B., Brown, P.L., Davis, J.A., Ekberg, C.,
1096 Kulik, D.A., Lutzenkirchen, J., Missana, T., Tachi, Y., Van Loon, L.R., and
1097 Altmann, S. (2013) Guidelines for thermodynamic sorption modelling in the
1098 context of radioactive waste disposal. Environmental Modelling & Software, 42,
1099 143-156.
1100 Pecini, E.M., and Avena, M.J. (2013) Measuring the isoelectric point of the edges of clay
1101 mineral particles: The case of montmorillonite. Langmuir, 29(48), 14926-14934.
1102 Rahromostaqim, M., and Sahimi, M. (2020) Molecular dynamics study of the effect of
1103 layer charge and interlayer cations on swelling of mixed-layer
1104 chlorite-montmorillonite clays. Journal of Physical Chemistry C, 124(4),
1105 2553-2561.
1106 Ramos-Tejada, M.M., de Vicente, J., Ontiveros, A., and Duran, J.D.G. (2001) Effect of
1107 humic acid adsorption on the rheological properties of sodium montmorillonite
1108 suspensions. Journal of Rheology, 45(5), 1159-1172.
1109 Rozalen, M., Brady, P.V., and Huertas, F.J. (2009) Surface chemistry of
1110 K-montmorillonite: Ionic strength, temperature dependence and dissolution
1111 kinetics. Journal of Colloid and Interface Science, 333(2), 474-484.
1112 Schindler, M., Legrand, C.A., and Hochella, M.F. (2015) Alteration, adsorption and
1113 nucleation processes on clay–water interfaces: Mechanisms for the retention of
1114 uranium by altered clay surfaces on the nanometer scale. Geochimica et
1115 Cosmochimica Acta, 153, 15-36.

1116 Schlegel, M.L., and Descostes, M. (2009) Uranium uptake by hectorite and
1117 montmorillonite: A solution chemistry and polarized EXAFS study.
1118 Environmental Science & Technology, 43(22), 8593-8598.
1119 Schlegel, M.L., and Manceau, A. (2006) Evidence for the nucleation and epitaxial growth
1120 of Zn phyllosilicate on montmorillonite. Geochimica et Cosmochimica Acta,
1121 70(4), 901-917.
1122 Schlegel, M.L., and Manceau, A. (2013) Binding mechanism of Cu(II) at the clay–water
1123 interface by powder and polarized EXAFS spectroscopy. Geochimica et
1124 Cosmochimica Acta, 113, 113-124.
1125 Schultz, C., and Grundl, T. (2004) pH dependence of ferrous sorption onto two smectite
1126 clays. Chemosphere, 57(10), 1301-1306.
1127 Secor, R.B., and Radke, C.J. (1985) Spillover of the diffuse double layer on
1128 montmorillonite particles. Journal of Colloid and Interface Science, 103, 237-244.
1129 Seif, S., Marofi, S., and Mahdavi, S. (2019) Removal of Cr3+ ion from aqueous solutions
1130 using MgO and montmorillonite nanoparticles. Environmental Earth Sciences,
1131 78(13), 377.
1132 Shi, J., Liu, H., Lou, Z., Zhang, Y., Meng, Y., Zeng, Q., and Yang, M. (2013) Effect of
1133 interlayer counterions on the structures of dry montmorillonites with Si^{4+}/Al^{3+}
1134 substitution. Computational Materials Science, 69, 95-99.
1135 Simonnin, P., Marry, V., Noetinger, B., Nieto-Draghi, C., and Rotenberg, B. (2018)
1136 Mineral- and ion-specific effects at clay–water interfaces: Structure, diffusion, and
1137 hydrodynamics. The Journal of Physical Chemistry C, 122(32), 18484-18492.

1138 Soltermann, D., Marques Fernandes, M., Baeyens, B., Dahn, R., Joshi, P.A., Scheinost,
1139 A.C., and Gorski, C.A. (2014) Fe(II) uptake on natural montmorillonites. I.
1140 Macroscopic and spectroscopic characterization. Environmental Science &
1141 Technology, 48(15), 8688-8697.
1142 Sposito, G., Holtzclaw, K.M., Jouany, C., and Charlet, L. (1983) Cation selectivity in
1143 sodium–calcium, sodium–magnesium and calcium–magnesium exchange on
1144 Wyoming bentonite at 298 K. Soil Science Society of America Journal, 47,
1145 917-921.
1146 Sposito, G., Skipper, N.T., Sutton, R., Park, S.H., Soper, A.K., and Greathouse, J.A.
1147 (1999) Surface geochemistry of the clay minerals. Proceedings of the National
1148 Academy of Sciences of the United States of America, 96(7), 3358-3364.
1149 Stephen Stackhouse, and Coveney, P.V. (2002) Study of thermally treated lithium
1150 montmorillonite by Ab Initio methods. Journal of Physical Chemistry B, 106,
1151 12470-12477.
1152 Sugiura, Y., Ishidera, T., and Tachi, Y. (2021) Surface complexation of Ca and
1153 competitive sorption of divalent cations on montmorillonite under alkaline
1154 conditions. Applied Clay Science, 200, 105910.
1155 Tahir, S.S., and Rauf, N. (2003) Thermodynamic studies of Ni(II) adsorption onto
1156 bentonite from aqueous solution. The Journal of Chemical Thermodynamics,
1157 35(12), 2003-2009.
1158 Tan, X.L., Hu, J., Montavon, G., and Wang, X.K. (2011) Sorption speciation of nickel(II)
1159 onto Ca-montmorillonite: Batch, EXAFS techniques and modeling. Dalton
1160 Transactions, 40(41), 10953-10960.

1161 Tazi, S., Rotenberg, B., Salanne, M., Sprik, M., and Sulpizi, M. (2012) Absolute acidity
1162 of clay edge sites from ab-initio simulations. Geochimica et Cosmochimica Acta,
1163 94, 1-11.
1164 Teich-McGoldrick, S.L., Greathouse, J.A., Jové-Colón, C.F., and Cygan, R.T. (2015)
1165 Swelling properties of montmorillonite and beidellite clay minerals from
1166 molecular simulation: Comparison of temperature, interlayer cation, and charge
1167 location effects. The Journal of Physical Chemistry C, 119(36), 20880-20891.
1168 Tertre, E., Berger, G., Castet, S., Loubet, M., and Giffaut, E. (2005) Experimental
1169 sorption of Ni^{2+}, Cs^{+} and Ln^{3+} onto a montmorillonite up to 150°C. Geochimica et
1170 Cosmochimica Acta, 69(21), 4937-4948.
1171 Tertre, E., Berger, G., Simoni, E., Castet, S., Giffaut, E., Loubet, M., and Catalette, H.
1172 (2006) Europium retention onto clay minerals from 25 to 150°C: Experimental
1173 measurements, spectroscopic features and sorption modelling. Geochimica et
1174 Cosmochimica Acta, 70(18), 4563-4578.
1175 Tombacz, E., and Szekeres, M. (2004) Colloidal behavior of aqueous montmorillonite
1176 suspensions: The specific role of pH in the presence of indifferent electrolytes.
1177 Applied Clay Science, 27(1-2), 75-94.
1178 Tournassat, C., Bizi, M., Braibant, G., and Crouzet, C. (2011) Influence of
1179 montmorillonite tactoid size on Na-Ca cation exchange reactions. Journal of
1180 Colloid and Interface Science, 364(2), 443-454.
1181 Tournassat, C., Bourg, I.C., Steefel, C.I., and Bergaya, F. (2015) Surface properties of
1182 clay minerals. Natural and Engineered Clay Barriers, p. 5-31.

1183 Tournassat, C., Davis, J.A., Chiaberge, C., Grangeon, S., and Bourg, I.C. (2016)
1184 Modeling the acid-base properties of montmorillonite edge surfaces.
1185 Environmental Science & Technology, 50(24), 13436-13445.
1186 Tournassat, C., Ferrage, E., Poinsignon, C., and Charlet, L. (2004) The titration of clay
1187 minerals II. Structure-based model and implications for clay reactivity. Journal of
1188 Colloid and Interface Science, 273(1), 234-246.
1189 Tournassat, C., Grangeon, S., Leroy, P., and Giffaut, E. (2013) Modeling specific pH
1190 dependent sorption of divalent metals on montmorillonite surfaces. A review of
1191 pitfalls, recent achievements and current challenges. American Journal of Science,
1192 313(5), 395-451.
1193 Tournassat, C., Tinnacher, R.M., Grangeon, S., and Davis, J.A. (2018) Modeling
1194 uranium(VI) adsorption onto montmorillonite under varying carbonate
1195 concentrations: A surface complexation model accounting for the spillover effect
1196 on surface potential. Geochimica et Cosmochimica Acta, 220, 291-308.
1197 Tran, E.L., Teutsch, N., Klein-BenDavid, O., and Weisbrod, N. (2018) Uranium and
1198 Cesium sorption to bentonite colloids under carbonate-rich environments:
1199 Implications for radionuclide transport. Science of the Total Environment, 643,
1200 260-269.
1201 Uddin, M.K. (2017) A review on the adsorption of heavy metals by clay minerals, with
1202 special focus on the past decade. Chemical Engineering Journal, 308, 438-462.
1203 van Genuchten, C.M., and Peña, J. (2016) Antimonate and arsenate speciation on reactive
1204 soil minerals studied by differential pair distribution function analysis. Chemical
1205 Geology, 429, 1-9.

1206 Van Groeningen, N., Gluck, B., Christl, I., and Kretzschmar, R. (2020) Surface
1207 precipitation of Mn^{2+} on clay minerals enhances Cd^{2+} sorption under anoxic
1208 conditions. Environmental Science-Processes & Impacts, 22(8), 1654-1665.
1209 Vao-soongnern, V., Pipatpanukul, C., and Horpibulsuk, S. (2015) A combined X-ray
1210 absorption spectroscopy and molecular dynamic simulation to study the local
1211 structure potassium ion in hydrated montmorillonite. Journal of Materials Science,
1212 50(21), 7126-7136.
1213 Voegelin, A., Wick, S., Pfenninger, N., Mangold, S., Baeyens, B., and Fernandes, M.M.
1214 (2022) Thallium adsorption onto phyllosilicate minerals. Environmental Science:
1215 Processes & Impacts, 24, 1343-1359.
1216 Wanner, H., Albinsson, Y., Karnland, O., Wieland, E., Wersin, P., and Charlet, L. (1994)
1217 The acid/base chemistry of montmorillonite. Radiochimica Acta, 66-7, 157-162.
1218 Whittaker, M.L., Lammers, L.N., Carrero, S., Gilbert, B., and Banfield, J.F. (2019) Ion
1219 exchange selectivity in clay is controlled by nanoscale chemical-mechanical
1220 coupling. Proceedings of the National Academy of Sciences of the United States
1221 of America, 116(44), 22052-22057.
1222 Wungu, T.D., Aspera, S.M., David, M.Y., Dipojono, H.K., Nakanishi, H., and Kasai, H.
1223 (2011) Absorption of lithium in montmorillonite: A density functional theory
1224 (DFT) study. Journal of Nanoscience and Nanotechnology, 11(4), 2793-801.
1225 Xu, D (2008) Adsorption of Pb(II) from aqueous solution to MX-80 bentonite: Effect of
1226 pH, ionic strength, foreign ions and temperature. Applied Clay Science, 41(1-2),
1227 37-46.

1228 Yang, S., Li, X., Jia, Z.Q., Li, Q.y., and Yang, G. (2018) Molecular dynamics simulations
1229 for the co-adsorption of binary electrolytes at the interface of montmorillonite and
1230 aqueous solutions. Soil Science Society of America Journal, 82(6), 1384-1391.
1231 Yang, S., Li, X., Li, Q.Y., Gu, P.K., Liu, X.T., and Yang, G. (2020) Competitive
1232 adsorption of metal ions at smectite/water interfaces: Mechanistic aspects, and
1233 impacts of co-ions, charge densities, and charge locations. Journal of Physical
1234 Chemistry C, 124(2), 1500-1510.
1235 Yang, S., Liu, X.T., and Yang, G. (2021) Thermodynamic and kinetic understanding of
1236 cation exchange at montmorillonite interfaces, and strong coupling with
1237 confinement effects. Applied Clay Science, 215, 106305.
1238 Yang, Y., Narayanan Nair, A.K., and Sun, S.Y. (2019) Layer charge effects on adsorption
1239 and diffusion of water and ions in interlayers and on external surfaces of
1240 montmorillonite. ACS Earth and Space Chemistry, 3(11), 2635-2645.
1241 Yu, S.J., Wang, X.X., Chen, Z.S., Tan, X.L., Wang, H.Q., Hu, J., Alsaedi, A., Alharbi,
1242 N.S., Guo, W., and Wang, X.K. (2016) Interaction mechanism of radionickel on
1243 Na-montmorillonite: Influences of pH, electrolyte cations, humic acid and
1244 temperature. Chemical Engineering Journal, 302, 77-85.
1245 Zhang, C., Liu, L.B., Dai, Y.C., Zhu, K.C., Liu, Z., and Jia, H.Z. (2022) Molecular
1246 dynamics simulations of exchange behavior of radionuclides into montmorillonite:
1247 Unraveling the dynamic processes and microscopic structures. Applied Clay
1248 Science, 226, 106579.
1249 Zhang, C., Liu, X.D., Lu, X.C., and He, M.J. (2018a) Complexation of heavy metal
1250 cations on clay edges at elevated temperatures. Chemical Geology, 479, 36-46.

1251 Zhang, C., Liu, X.D., Lu, X.C., He, M.J., Meijer, E.J., and Wang, R.C. (2017) Surface
1252 complexation of heavy metal cations on clay edges: Insights from first principles
1253 molecular dynamics simulation of Ni(II). Geochimica et Cosmochimica Acta, 203,
1254 54-68.
1255 Zhang, C., Liu, X.D., Lu, X.C., Meijer, E.J., Wang, K., He, M.J., and Wang, R.C. (2016)
1256 Cadmium(ii) complexes adsorbed on clay edge surfaces: Insight from first
1257 principles molecular dynamics simulation. Clays and Clay Minerals, 64(4),
1258 337-347.
1259 Zhang, C., Liu, X.D., Lu, X.C., Meijer, E.J., and Wang, R.C. (2019a) An atomic-scale
1260 understanding of the initial stage of nucleation of heavy metal cations on clay
1261 edges. Geochimica et Cosmochimica Acta, 248, 161-171.
1262 Zhang, C., Liu, X.D., Lu, X.C., Meijer, E.J., and Wang, R.C. (2019b) Understanding the
1263 heterogeneous nucleation of heavy metal phyllosilicates on clay edges with
1264 first-principles molecular dynamics. Environmental Science & Technology,
1265 53(23), 13704-13712.
1266 Zhang, C., Liu, X.D., Tinnacher, R.M., and Tournassat, C. (2018b) Mechanistic
1267 understanding of uranyl ion complexation on montmorillonite edges: A combined
1268 first-principles molecular dynamics-surface complexation modeling approach.
1269 Environmental Science & Technology, 52(15), 8501-8509.
1270 Zhang, W., Li, J.S., Chen, S.X., Huang, K., Luo, L.J., Tong, K.W., Guo, J.H., Li, S.C.,
1271 Zhang, R., and Dai, Z.J. (2023) Effect of layer charge density and cation
1272 concentration on sorption behaviors of heavy metal ions in the interlayer and

nanopore of montmorillonite: A molecular dynamics simulation. Colloids and Surfaces A: Physicochemical and Engineering Aspects, 657, 130553.

Zhu, J., Cozzolino, V., Pigna, M., Huang, Q.Y., Caporale, A.G., and Violante, A. (2011) Sorption of Cu, Pb and Cr on Na-montmorillonite: Competition and effect of major elements. Chemosphere, 84(4), 484-489.

Zhu, R.L., Chen, Q.Z., Zhou, Q., Xi, Y.F., Zhu, J.X., and He, H.P. (2016) Adsorbents based on montmorillonite for contaminant removal from water: A review. Applied Clay Science, 123, 239-258.

List of Figure Captions

Fig. 1 (A) Important implications of the Mt–cation interfacial interactions in the Earth science, environmental remediation, and industrial processes and (B) Schematic diagrams of the lattice structure of Mt.

Fig. 2 Modeling of metal cations adsorbed on Mt. (A) Quantification of metal cations adsorbed on Mt; (B) Cation exchange process; (C) Surface complexation process; (D) Electrostatic models of Mt surface/water surface. C_{init}: initial added concentration for the metal cation; C_{eq}: the concentration for the metal cation at the end of the equilibration period; R_{SL}: solid-to-liquid ratio ($m_{Mt}/V_{solution}$); *X*: exchange sites; ≡SOH: hydroxyl group on Mt surface; {i}: mass specific concentrations of surface species *i*; (i): activities; γ_{surf}: the activity coefficient of surface species; γ_i: aqueous solution activity coefficients; [i]: concentrations of aqueous species *i*; *F*: Faraday's constant (96,485 C mol^{-1}); *R*: the universal gas constant (8.314 J mol^{-1} K^{-1}); *T*: temperature; ψ_i: electrostatic potential of *i*.

Fig. 3 The adsorption sites and behaviors on Mt basal surface. (A) Schematic diagram of inner-sphere surface complexes (ISSC) and outer-sphere surface complexes (OSSC). (B) ISSC of K^+ on the surface basal plane. (C) Adsorption sites of Cs^+ on Mt basal surface. (D) The mobility of adsorbed K^+ as an inner-sphere complex (Adapted from Liu and Lu (2006) A thermodynamic understanding of clay-swelling inhibition by potassium ions. Angewandte Chemie International Edition, 45(38), 6300-6303. Copyright 2006, with permission from John Wiley and Sons).

Fig. 4 The structures of edge sites on AC and B edge surfaces and the associated pK_a values. (Adapted with permission from Tournassat et al. (2016) Modeling the acid-base

properties of montmorillonite edge surfaces. Environmental Science & Technology, 50(24), 13436-13445. Copyright 2016 American Chemical Society.).

Fig. 5 Interfacial interactions of metal cations adsorbed on Mt [010] and [110] edges. (A) Ni^{2+} adsorbed on ≡SiOH, ≡$Al(OH)_2$, and vacant sites on [010] edges, and (B) Ni^{2+} adsorbed on ≡SiOH, ≡(SiAl)OH, and vacant sites on [110] edges (Adapted from Zhang et al. (2017), Geochimica et Cosmochimica Acta, 203, 54-68. Copyright 2017, with permission from Elsevier.). (C) Cd^{2+}, Co^{2+}, Cu^{2+} and Pb^{2+} adsorbed on the vacant sites on Mt [010] edge; (Adapted from Zhang et al. (2017), Geochimica et Cosmochimica Acta, 203, 54-68. Copyright 2017, with permission from Elsevier; Adapted from Zhang et al. (2019a), Geochimica et Cosmochimica Acta, 248, 161-171. Copyright 2019, with permission from Elsevier.). (D) Uranyl adsorbed on Mt [010] and [110] edges. (Adapted with permission from Zhang et al. (2018b), Environmental Science & Technology, 52, 8501-8509. Copyright 2018 American Chemical Society.).

Fig. 6 Nucleation and precipitation processes of metal cations on Mt edge surfaces. (A) stepwise pathway and (B) Synchronous pathway. (Adapted with permission from Zhang et al. (2019b), Environmental Science & Technology, 53, 13704-13712. Copyright 2019 American Chemical Society.).

Fig. 7 The influence of pH and ionic strength on the adsorption behaviors. (A) Schematic diagram of metal cations adsorbed on Mt as a function of pH (Adapted with permission from Tournassat et al. (2013), American Journal of Science, 313, 395-451. Copyright 2013, with permission from American Journal of Science.); (B) The pH-dependent speciations of the related ionic forms and distribution; (C) The relative proportions of adsorbed Cd^{2+}, Cu^{2+}, Ni^{2+}, Pb^{2+}, and Zn^{2+} onto Na-Mt at different ionic strengths (i.e.,

0.001, 0.01, and 0.1 M of $NaNO_3$) and pH values); (Adapted from Gu et al. (2010), Geochimica et Cosmochimica Acta, 74, 5718-5728. Copyright 2010, with permission from Elsevier.). (D) Association pattern of Mt layers under different ionic strengths.

Fig. 8 The competitive adsorption behavior of Ca^{2+} in the presence of competition cations (i.e., Sr^{2+}, Ni^{2+}, and Pb^{2+}) on Mt edge surfaces. (A) Sr^{2+} adsorbed onto Na-Mt in the presence and absence of Ca^{2+}, (B) Ni^{2+} adsorbed onto Na-Mt in the presence and absence of Ca^{2+}. (Adapted with permission from Sugiura et al., (2021), Applied Clay Science, 200, 105910. Copyright 2021, with permission from Elsevier.). (C) Effect of the addition of Mg^{2+} on (C) Mt edge surface charge and (D) Pb^{2+} adsorption on edge surface. (Adapted with permission from Orucoglu et al., (2022), ACS Earth and Space Chemistry, 6, 144-159. Copyright 2022 American Chemical Society.).

Fig. 9 Effect of competing cations (Al^{3+}, Fe^{3+}, Ca^{2+} and Mg^{2+}) on the adsorption of heavy metal pollutants (Cu^{2+}, Pb^{2+} and Cr^{2+}) by Na-Mt with increasing concentration ratio of competing cations to target metal ($R_{m/h}$) from 0 to 15: (A) Cu at pH 3.5, (B) Cu at pH 4.5, (C) Cu at pH 5.5, (D) Pb at pH 3.5, (E) Pb at pH 4.5, (F) Pb at pH 5.5, (G) Cr at pH 3.5, (H) Cr at pH 4.5, and (I) Cr at pH 5.5. (Adapt with permission from Zhu et al., (2011), Chemosphere, 84, 484-489. Copyright 2011, with permission from Elsevier.).

Fig. 10 Impact of competing cations on Ra^{2+} adsorption. The concentrations of NaCl, KCl, $CaCl_2$, $MgCl_2$, and $SrCl_2$ are all 10 mM, AGW (artificial groundwater) is composed of elements, such as Na (5 mM), K (2 mM), Mg (0.5 mM), Ca (0.5 mM), Sr (0.0001 mM), and Cl (9 mM). (Adapted with permission from Chen and Kocar, (2018), Environmental Science & Technology, 52, 4023-4030. Copyright 2018 American Chemical Society.).

Fig. 11 Temperature dependency of the cation adsorption processes. (A) Effect of temperature on (A) diffusion coefficient, (B) hydration state, and (C) the adsorption energy of Pb^{2+} ion (C_i: initial Pb^{2+} concentration; H_1: first peak value of radial distribution function curve of Pb^{2+} to water oxygen; C_e: maximum initial Pb^{2+} concentration identified by adsorption energy) (Adapted with permission from Du et al., (2022), Environmental Research, 209, 112817. Copyright 2022, with permission from Elsevier.). (D) Adsorption behavior of metal cations on Mt basal surface at 298, 373, and 423 K. (Adapted with permission from Zhang et al., (2022), Applied Clay Science, 226, 106579. Copyright 2022, with permission from Elsevier.).

Fig. 12 The influence of layer charge density and location on the cation exchange process. (A) The density distributions of Pb^{2+}, Ba^{2+}, and Cs^{+} and water oxygen atoms on surface basal plane (Adapted with permission from Zhang et al., (2023), Colloids and Surfaces A: Physicochemical and Engineering Aspects, 657, 130553. Copyright 2023, with permission from Elsevier.). (B) Atomic density profiles of Zn^{2+}, Cd^{2+}, and Pb^{2+} cations along the direction perpendicular to Arizona and Wyoming Mt basal surfaces and (C) Time-evolution trajectories of the adsorbed heavy metal cations at basal surfaces of Arizona and Wyoming Mt. (Adapted with permission from Liu et al., (2021), Journal of Hazardous Materials, 416, 125976. Copyright 2021, with permission from Elsevier.).

Fig. 13 Electrostatic spillover effect of Mt layer related to the stacking modes and ionic strengths. (A) 2D geometry considered for solving the Poisson-Boltzmann equation (zoom on the edge surface region) in three different geometries. (B) The edge potential as a function of edge charge for three ionic strengths (0.001, 0.01, and 0.1) at the arrow position in panel A. (Adapted with permission from Tournassat et al., (2013), American

1372 Journal of Science, 313, 395-451. Copyright 2013, with permission from American
1373 Journal of Science.).
1374
1375

1376

Table 1. Adsorption sites of metal cations on basal surface of Mt

Cations	Montmorillonite	Chemical environment of adsorption sites	Methods	Reference
Li^+	$Li[Si_8][Al_3Mg]O_{20}(OH)_4$	Cations prefer to occupy vacant octahedral sites than the ditrigonal cavities of tetrahedral sheet.	XRD/MD	(Hrobáriková et al., 2001; Stephen Stackhouse and Coveney, 2002; Wungu et al., 2011)
	Na-Mt with Si^{4+}/Al^{3+} substitution	Cations occupy the siloxane cavities on the basal plane and form strong bonds to the oxygens of the Al-substituted tetrahedral.	DFT	(Shi et al., 2013)
Na^+	Na-Mt with Si^{4+}/Al^{3+} substitution	Cations occupy the siloxane cavities on the basal plane and form strong bonds to the oxygens of the Al-substituted tetrahedral.	DFT	(Shi et al., 2013)
K^+	$Na[Si_8][Al_3Mg]O_{20}(OH)_4$	Cations are tightly confined in coordination cages above surface hexagons	MD	(Liu and Lu, 2006)
	Na-Mt with Si^{4+}/Al^{3+} substitution	Cations occupy the siloxane cavities on the basal plane and form strong bonds to the oxygens of the Al-substituted tetrahedral.	DFT	(Shi et al., 2013)
Cs^+	$[Na_{0.64}K_{0.01}H_{0.04}Mg_{0.01}Ca_{0.07}][Al_{3.35}Mg_{0.5}Fe_{0.09}{}^{3+}Fe_{0.06}{}^{2+}][Si_{7.61}Al_{0.39}]O_{20}(OH)_4$	At low Cs exchange fractions, the preferred adsorption site is the center of the hexagonal cavities including Al substitution. For higher Cs exchange fractions, the other two locations (i.e., center of the hexagonal cavities that do not include Al and the surface on the open nanospace) can be new adsorption sites.	NMR/DFT	(Ohkubo et al., 2018)
Mg^{2+}	Na-Mt with Si^{4+}/Al^{3+} substitution	Cations occupy the siloxane cavities on the basal plane and form strong bonds to the oxygens of the Al-substituted tetrahedral.	DFT	(Shi et al., 2013)
Ca^{2+}	Na-Mt with Si^{4+}/Al^{3+} substitution	Cations occupy the siloxane cavities on the basal plane and form strong bonds to the oxygens of the Al-substituted tetrahedral.	DFT	(Shi et al., 2013)

1377

1378

1379

1380

1381

1382

1383

This is the peer-reviewed, final accepted version for American Mineralogist, published by the Mineralogical Society of America.
The published version is subject to change. Cite as Authors (Year) Title. American Mineralogist, in press.
DOI: https://doi.org/10.2138/am-2022-8834. http://www.minsocam.org/

1384

Table 2. Adsorption sites of metal cations on edge surface of Mt

Cations	Montmorillonite	Chemical environment of adsorption sites	Methods	Reference
Ni^{2+}	$[Si_8][Al_4Mg]O_{20}(OH)_4$	Cations form tetradentate complexes on the octahedral vacant site (strong site), but Ni^{2+} occupies lattice positions. Cations form monodentate complexes on the ≡SiOH and bidentate complexes on the ≡$Al(OH)_2$ sites for [010] edges or ≡AlOH≡AlSiO sites for [110] edges (weak site).	FPMD	(Zhang et al., 2017, 2018a)
Cu^{2+}	$[Si_8][Al_4Mg]O_{20}(OH)_4$	Cations are penta-coordinated on the octahedral vacant site (strong site).	FPMD	(Zhang et al., 2017)
Zn^{2+}	Milos and STx-1 Mt	At low loading, Zn^{2+} was incorporated into the outermost trans-octahedra (strong site). At medium loading, Zn^{2+} formed monodentate and bidentate inner-sphere surface complexes on the [010] and [110] edges (weak site).	EXAFS/MD	(Churakov and Dähn, 2012)
Pb^{2+}	$[Si_8][Al_4]O_{20}(OH)_4$	Cations formed bidentate complex on the octahedral vacant site, the ≡$Al(OH)_2$ site and the ≡SiO site with the similar probability.	FPMD	(Zhang et al., 2019a)
Cd^{2+}	$[Si_8][Al_4Mg]O_{20}(OH)_4$	Cations form tetradentate complex on the octahedral vacant site (strong site), but Cd^{2+} does not occupy the lattice position. Cations form monodentate complexes on the ≡SiO and bidentate complexes on the ≡$Al(OH)_2$ site for [010] edges or≡AlOH≡AlSiO sites for [110] edges (weak site).	FPMD	(Zhang et al., 2016, 2017, 2018a)
Co^{2+}	$[Si_8][Al_4Mg]O_{20}(OH)_4$	Cations form tetradentate complexes on the octahedral vacant site (strong site).	FPMD	(Zhang et al., 2017)
Fe^{2+}	$[Si_8][Al_4Mg]O_{20}(OH)_4$ $Li_{0.5}[Si_8][Al_{3.5}Mg_{0.5}]O_{20}(OH)_4$	Cations form bidentate complexes on ≡Al-OH sites of Mt [010] edge and [110] ≡Al-O-Si≡ site, and monodentate complexes on ≡SiOH sites of Mt [010] edge and [110] ≡Si-O- site are most stable sites.	FPMD	(Liu et al., 2012a, 2013a)
Sb (V)		Cations form a bidentate complex attached to the edges of the octahedral sheet.	PDF	(van Genuchten and Peña, 2016)
Eu/Cm/Am	Na-Mt	At low loadings, cations form strong inner-sphere complexes through binding to three Al octahedron, most likely by occupying vacant sites in the octahedral layers of Mt, which are exposed on [010] and [110] edge faces. At higher loadings, cations binds to only one Al octahedron, forming a weaker, edge-sharing surface complex.	EXAFS and TRLFS	(Marques Fernandes et al., 2016)
Am	GMZ bentonite	At the sites of ≡$Al(OH)_2$ on [010] surface and ≡AlO(OH) on [110] surface are bidentate.	DFT	(Gao et al., 2021)
U	$Li_{0.5}[Si_8][Al_{3.5}Mg_{0.5}]O_{20}(OH)_4$ $Na_q(Si_{4-n}Al_n)(Al_{2-m}Mg_m)O_{10}(OH)_2$	UO_2^{2+} forms bidentate complexes at ≡$Al(OH)_2$ and ≡AlOHSiO on the [010] surface and ≡AlOHO and ≡SiOH on the [110] surface.	FPMD	(Kremleva et al., 2015; Zhang et al., 2018b)
La	Ca-Mt, Na-Mt	Cations prefer to form mono-or bi-dentate inner-sphere complexes at lower La loadings.	EXAFS/XANES	(Lepore et al., 2022)

1385

1386

1387

1388

1389

This is the peer-reviewed, final accepted version for American Mineralogist, published by the Mineralogical Society of America.
The published version is subject to change. Cite as Authors (Year) Title. American Mineralogist, in press.
DOI: https://doi.org/10.2138/am-2022-8834. http://www.minsocam.org/

1390

1391

Table 3. Thermodynamic data of metal cations adsorbed on Mt.

Cation	Montmorillonite	Range of temperature (K)	Δ*H* (kJ/mol)	Δ*S* (J/mol/K)	-ΔG (kJ/mol)	Reference
Cs^{+}	Purified MX-80 bentonite	298-423	-19±5	/	/	(Tertre et al., 2005)
	Barmer bentonite	298-328	−14.25	31.39	23.5-25.5	(Gupt et al., 2020)
Pb^{2+}	MX-80 bentonite	291-328	−19.77	−10.22		(Xu, 2008)
	Mt is calcined at 773 K for 10 h	303-313	−75.5	−235.9	71.4-73.8	(Bhattacharyya and Gupta, 2007)
	Mt is calcined at 773 K for 10 h	303-313	−45.1	−146.4	44.4-45.9	(Bhattacharyya, 2008; Bhattacharyya and Gupta, 2007)
	Ugwuoba montmorillonite	300-323	17.23	62.27	1.5-2.9	(Akpomie et al., 2015)
Ni^{2+}	Na-montmorillonite	298-328	15.57	60.87	2.5-4.4	(Yu et al., 2016)
	Purified MX-80 bentonite	298-423	33±10	/	/	(Tertre et al., 2005)
	bentonite	298-323	0.82-2.59	0.032-0.033	7.1-10.7	(Tahir and Rauf, 2003)
Cd^{2+}	Mt is calcined at 773 K for 10 h	303-313	40.2	147.5	44.6-46.1	(Bhattacharyya and Gupta, 2007)
Co^{2+}	Mt is calcined at 773 K for 10 h	303-313	−15.1	−47.1	14.3-14.7	(Bhattacharyya, 2008; Bhattacharyya and Gupta, 2007)
Cu^{2+}	Mt is calcined at 773 K for 10 h	303-313	50.7	180.7	54.7-55.9	(Bhattacharyya and Gupta, 2007)
Mn^{2+}	Ugwuoba montmorillonite	300-323	15.19	52.00	0.48-1.65	(Akpomie et al., 2015)
Cr^{3+}	/	288-308	-7.23	-40.44	−2.1 - -8.0	(Seif et al., 2019)
Fe^{3+}	Mt is calcined at 773 K for 10 h	303-313	−27.6	−86.6	26.2-27.2	(Bhattacharyya, 2008)
Eu^{3+}	Purified MX-80 bentonite	298-423	39±15	/	/	(Tertre et al., 2005)

1392

1393

1394

1395

1396

1397

1398

1399

This is the peer-reviewed, final accepted version for American Mineralogist, published by the Mineralogical Society of America.
The published version is subject to change. Cite as Authors (Year) Title. American Mineralogist, in press.
DOI: https://doi.org/10.2138/am-2022-8834. http://www.minsocam.org/

1400

1401 **Table 4. The distribution of adsorbed cations through cation exchange on Mt basal surface as a function of layer charge densities and localization**

Composition of Mt	Layer charge (e.uc^{-1})		Cation	Cation distribution	Reference
	Octahedral charge	Tetrahedral charge			
$Na[Al_3Mg][Si_8]O_{20}(OH)_4$	-1.0	0	Na^+	mostly form ISSC at monolayer hydrated state, and OSSC at bilayer hydrated state	(Yang et al., 2019; Li et al., 2020; Ghasemi and Sharifi, 2021)
$Na_{0.75}[Al_{3.5}Mg_{0.5}][Si_{7.75}Al_{0.25}]O_{20}(OH)_4$	-0.5	-0.25	Na^+	the fraction of ISSC decreased from 100% to 0% while the OSSC increased from 0% to 100% with increasing RH	(Churakov, 2013; Li et al., 2019b; Yang et al., 2019; Li et al., 2020; Rahromostaqim and Sahimi, 2020; Ghasemi and Sharifi, 2021)
$Na_{0.75}[Al_{3.5}Mg_{0.5}][Si_{7.75}Al_{0.25}]O_{20}(OH)_4$	-0.5	-0.25	K^+	almost always form ISSC	(Li et al., 2019b; Yang et al., 2019; Rahromostaqim and Sahimi, 2020)
			Cs^+	the fraction of ISSC decreased from 100% to31% while the OSSC increased form 0% to 69% with increasing RH	(Churakov, 2013; Rahromostaqim and Sahimi, 2020)
$M_{1.0/n}[Al_3Mg][Si_8]O_{20}(OH)_4$	-1.0	0	Li^+	mostly form ISSC at monolayer hydrated state and partially OSSC at bilayer hydrated state	(Yang et al., 2019)
			K^+	almost always form ISSC	
			Ca^{2+}	almost always form OSSC	
			Mg^{2+}	almost always form OSSC	
			Sr^{2+}	mostly form ISSC at RH < 10%, and almost always form OSSC at RH > 50%	
			Li^+	almost always form ISSC at RH < 50%, and mostly form OSSC at RH > 90%.	
$M_{0.75/n}[Al_{3.5}Mg_{0.5}][Si_{7.75}Al_{0.25}]O_{20}(OH)_4$	-0.5	-0.25	Ca^{2+}	almost always form OSSC	(Li et al., 2019b; Yang et al., 2019)
			Mg^{2+}	mostly form ISSC at RH < 10% and almost always form OSSC at RH > 50%.	
			Sr^{2+}	almost always form ISSC at RH < 10% and almost always form OSSC at RH > 50%	
$M_{1.0/n}[Al_3Mg][Si_8]O_{20}(OH)_4$	-1.0	0	Zn^{2+} Cd^{2+} Pb^{2+}	only form OSSC	(Liu et al., 2021)
$M_{1.0/n}[Al_{3.33}Mg_{0.67}][Si_{7.67}Al_{0.33}]O_{20}(OH)_4$	0.67	0.33	Zn^{2+}	only form OSSC	
			Cd^{2+} Pb^{2+}	both cations form ISSC and OSSC	

1402

This is the peer-reviewed, final accepted version for American Mineralogist, published by the Mineralogical Society of America.
The published version is subject to change. Cite as Authors (Year) Title. American Mineralogist, in press.
DOI: https://doi.org/10.2138/am-2022-8834. http://www.minsocam.org/

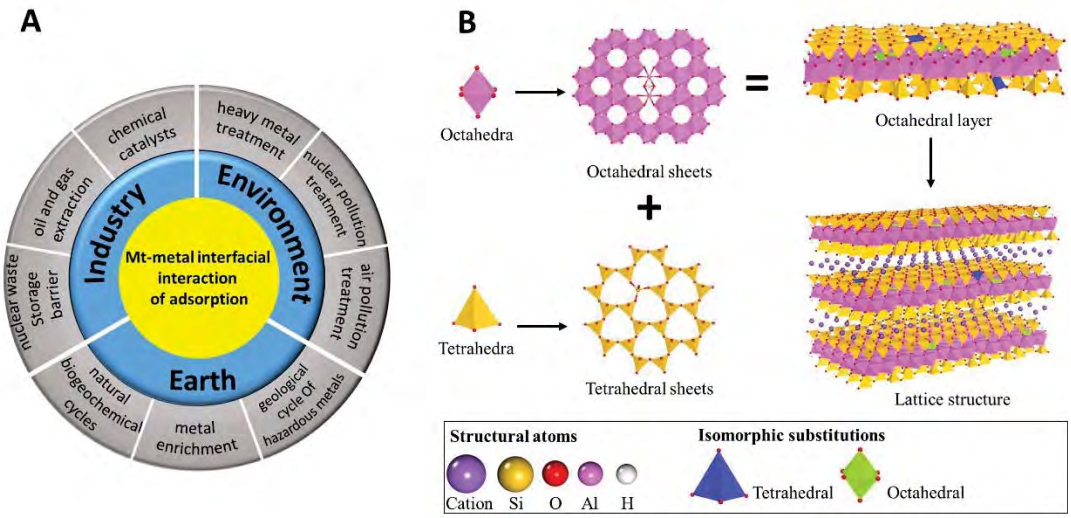

Fig. 1 (A) Important implications of the Mt–cation interfacial interactions in the Earth science, environmental remediation, and industrial processes and (B) Schematic diagrams of the lattice structure of Mt.

This is the peer-reviewed, final accepted version for American Mineralogist, published by the Mineralogical Society of America.
The published version is subject to change. Cite as Authors (Year) Title. American Mineralogist, in press.
DOI: https://doi.org/10.2138/am-2022-8834. http://www.minsocam.org/

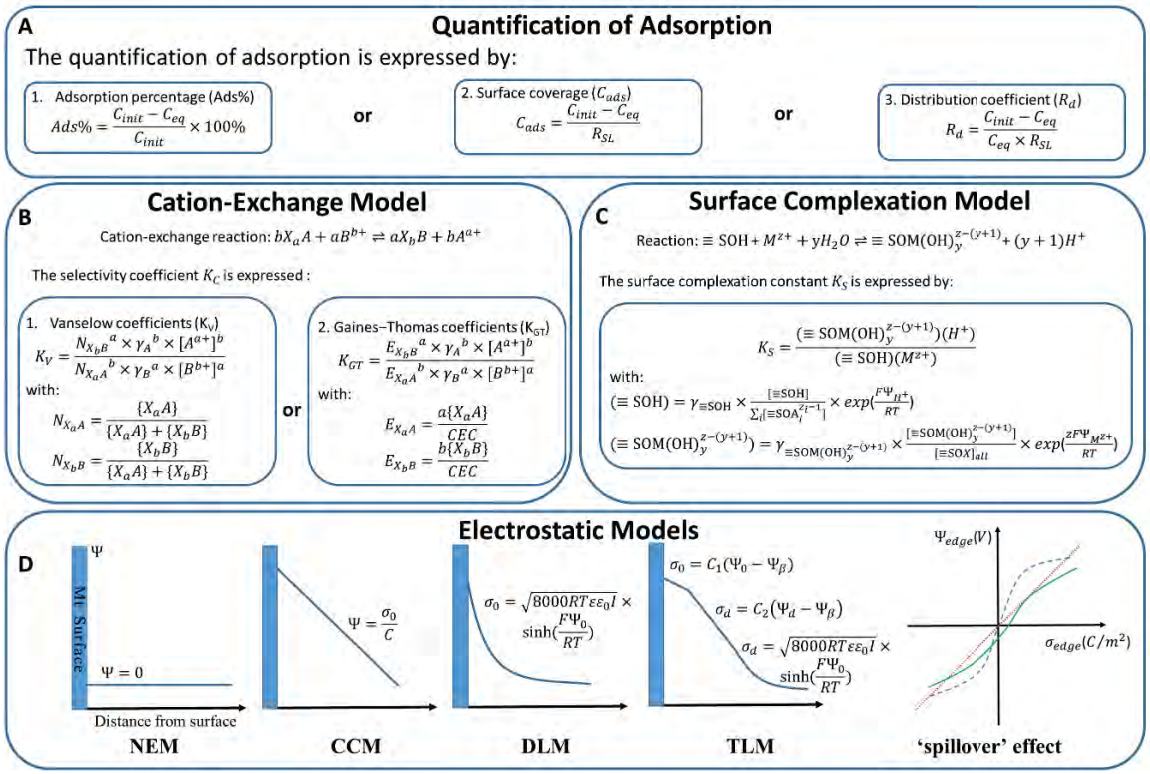

Fig. 2 Modeling of metal cations adsorbed on Mt. (A) Quantification of metal cations adsorbed on Mt; (B) Cation exchange process; (C) Surface complexation process; (D) Electrostatic models of Mt surface/water surface. C_{init}: initial added concentration for the metal cation; C_{eq}: the concentration for the metal cation at the end of the equilibration period; R_{SL}: solid-to-liquid ratio ($m_{Mt}/V_{solution}$); X: exchange sites; ≡SOH: hydroxyl group on Mt surface; {i}: mass specific concentrations of surface species i; (i): activities; γ_{surf}: the activity coefficient of surface species; γ_i: aqueous solution activity coefficients; [i]: concentrations of aqueous species i; F: Faraday's constant (96,485 C mol^{-1}); R: the universal gas constant (8.314 J mol^{-1} K^{-1}); T: temperature; ψ_i: electrostatic potential of i.

This is the peer-reviewed, final accepted version for American Mineralogist, published by the Mineralogical Society of America.
The published version is subject to change. Cite as Authors (Year) Title. American Mineralogist, in press.
DOI: https://doi.org/10.2138/am-2022-8834. http://www.minsocam.org/

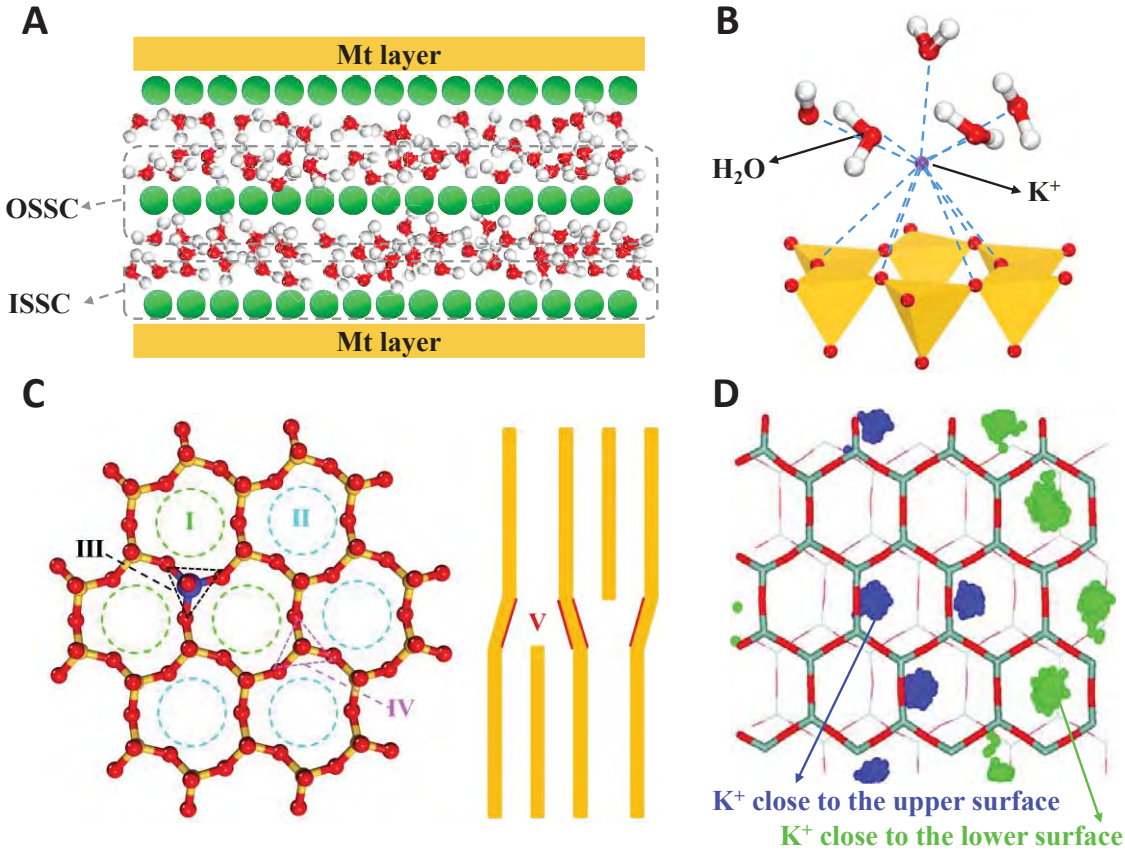

Fig. 3 The adsorption sites and behaviors on Mt basal surface. (A) Schematic diagram of inner-sphere surface complexes (ISSC) and outer-sphere surface complexes (OSSC). (B) ISSC of K^+ on the surface basal plane. (C) Adsorption sites of Cs^+ on Mt basal surface. (D) The mobility of adsorbed K^+ as an inner-sphere complex (Adapted from Liu and Lu (2006) A thermodynamic understanding of clay-swelling inhibition by potassium ions. Angewandte Chemie International Edition, 45(38), 6300-6303. Copyright 2006, with permission from John Wiley and Sons).

This is the peer-reviewed, final accepted version for American Mineralogist, published by the Mineralogical Society of America.
The published version is subject to change. Cite as Authors (Year) Title. American Mineralogist, in press.
DOI: https://doi.org/10.2138/am-2022-8834. http://www.minsocam.org/

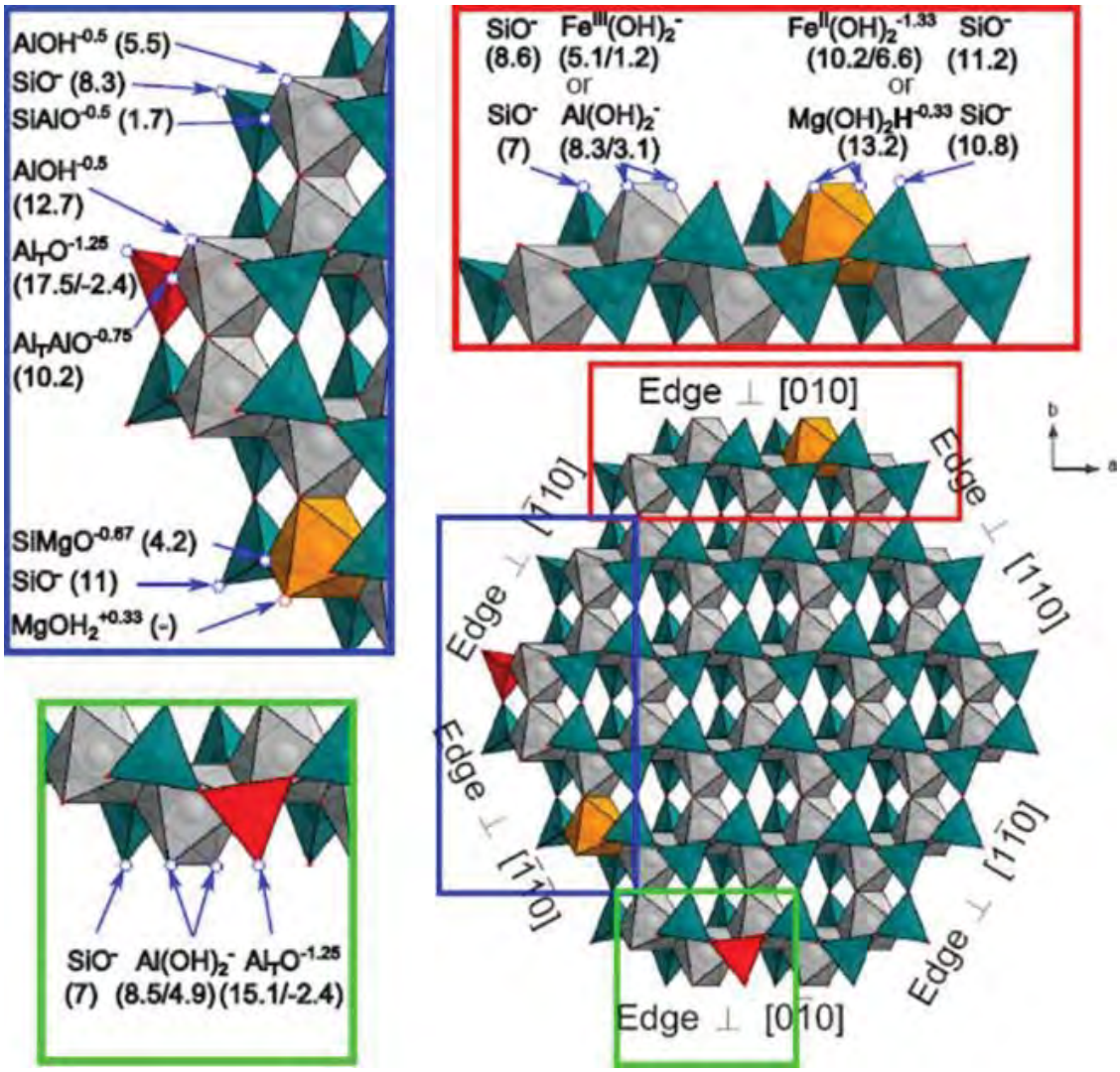

Fig. 4 The structures of edge sites on AC and B edge surfaces and the associated pK_a values. (Adapted with permission from Tournassat et al. (2016) Modeling the acid-base properties of montmorillonite edge surfaces. Environmental Science & Technology, 50(24), 13436-13445. Copyright 2016 American Chemical Society.).

This is the peer-reviewed, final accepted version for American Mineralogist, published by the Mineralogical Society of America.
The published version is subject to change. Cite as Authors (Year) Title. American Mineralogist, in press.
DOI: https://doi.org/10.2138/am-2022-8834. http://www.minsocam.org/

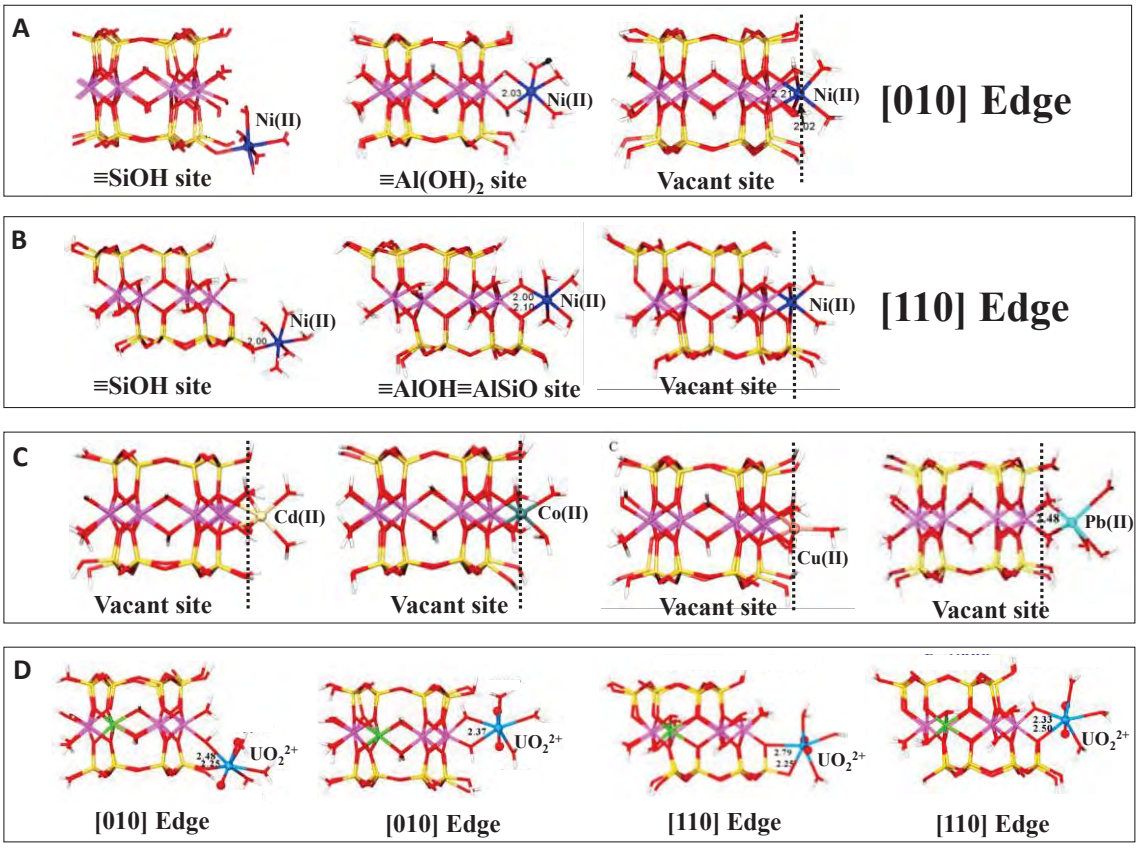

Fig. 5 Interfacial interactions of metal cations adsorbed on Mt [010] and [110] edges. (A) Ni^{2+} adsorbed on ≡SiOH, ≡$Al(OH)_2$, and vacant sites on [010] edges, and (B) Ni^{2+} adsorbed on ≡SiOH, ≡(SiAl)OH, and vacant sites on [110] edges (Adapted from Zhang et al. (2017), Geochimica et Cosmochimica Acta, 203, 54-68. Copyright 2017, with permission from Elsevier.). (C) Cd^{2+}, Co^{2+}, Cu^{2+} and Pb^{2+} adsorbed on the vacant sites on Mt [010] edge; (Adapted from Zhang et al. (2017), Geochimica et Cosmochimica Acta, 203, 54-68. Copyright 2017, with permission from Elsevier; Adapted from Zhang et al. (2019a), Geochimica et Cosmochimica Acta, 248, 161-171. Copyright 2019, with permission from Elsevier.). (D) Uranyl adsorbed on Mt [010] and [110] edges. (Adapted with permission

from Zhang et al. (2018b), Environmental Science & Technology, 52, 8501-8509. Copyright 2018 American Chemical Society.).

This is the peer-reviewed, final accepted version for American Mineralogist, published by the Mineralogical Society of America.
The published version is subject to change. Cite as Authors (Year) Title. American Mineralogist, in press.
DOI: https://doi.org/10.2138/am-2022-8834. http://www.minsocam.org/

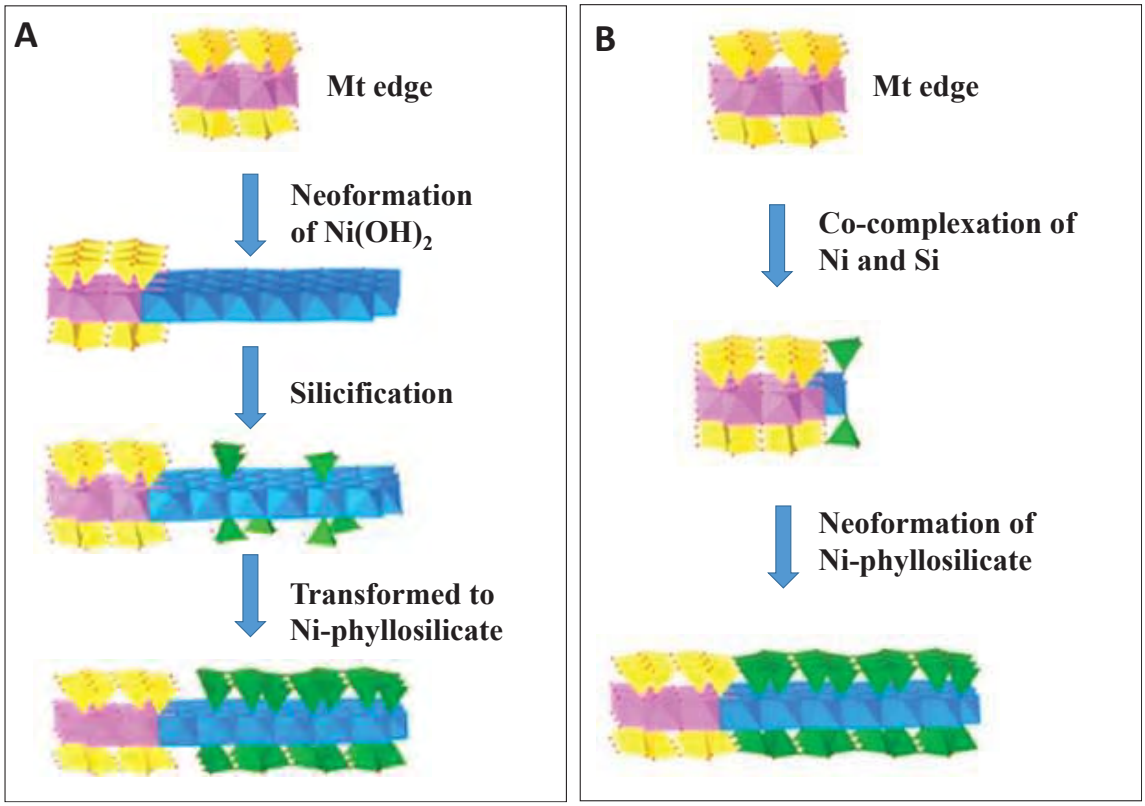

Fig. 6 Nucleation and precipitation processes of metal cations on Mt edge surfaces. (A) stepwise pathway and (B) Synchronous pathway. (Adapted with permission from Zhang et al. (2019b), Environmental Science & Technology, 53, 13704-13712. Copyright 2019 American Chemical Society.).

This is the peer-reviewed, final accepted version for American Mineralogist, published by the Mineralogical Society of America.
The published version is subject to change. Cite as Authors (Year) Title. American Mineralogist, in press.
DOI: https://doi.org/10.2138/am-2022-8834. http://www.minsocam.org/

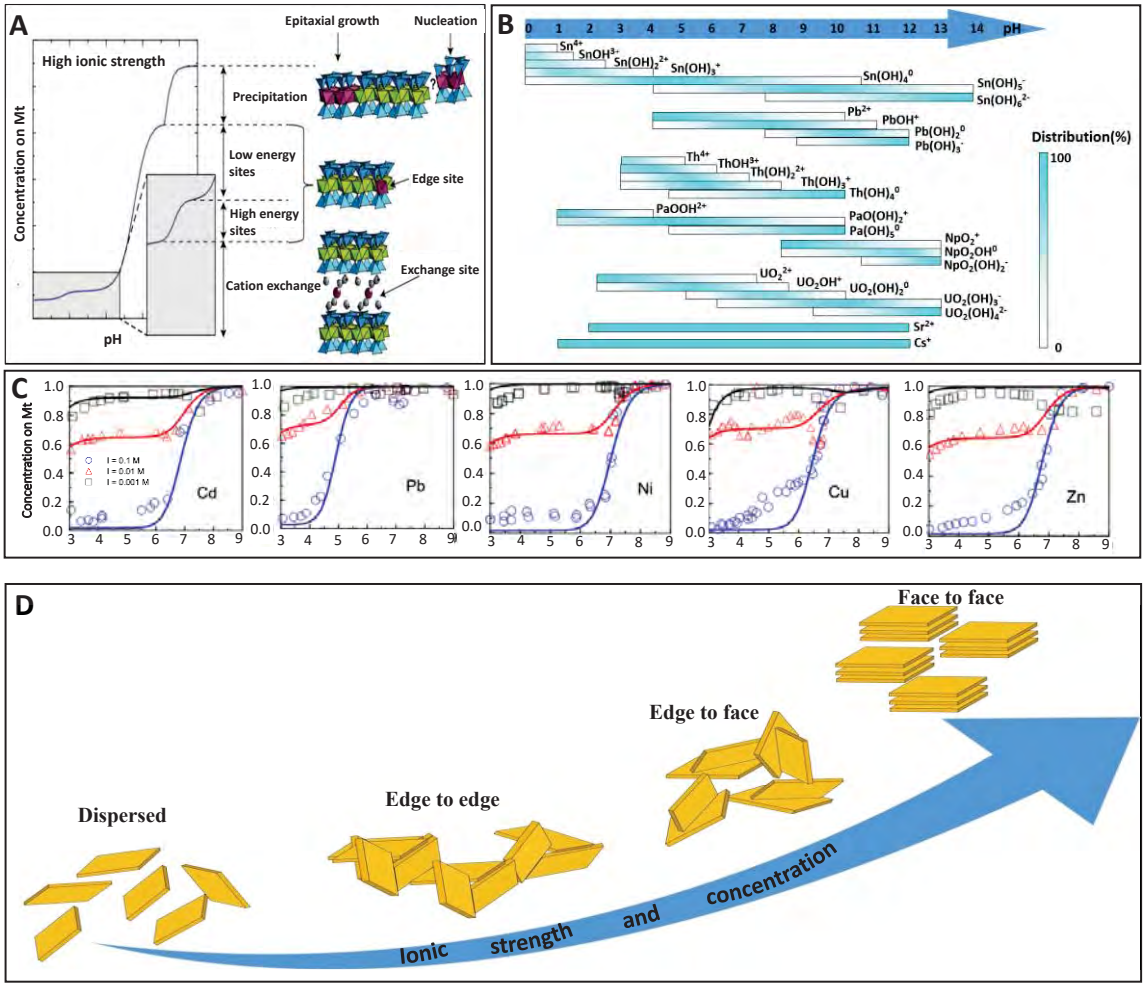

Fig. 7 The influence of pH and ionic strength on the adsorption behaviors. (A) Schematic diagram of metal cations adsorbed on Mt as a function of pH (Adapted with permission from Tournassat et al. (2013), American Journal of Science, 313, 395-451. Copyright 2013, with permission from American Journal of Science.); (B) The pH-dependent speciations of the related ionic forms and distribution; (C) The relative proportions of adsorbed Cd^{2+}, Cu^{2+}, Ni^{2+}, Pb^{2+}, and Zn^{2+} onto Na-Mt at different ionic strengths (i.e., 0.001, 0.01, and 0.1 M of $NaNO_3$) and pH values); (Adapted from Gu et al. (2010), Geochimica et

Cosmochimica Acta, 74, 5718-5728. Copyright 2010, with permission from Elsevier.). (D) Association pattern of Mt layers under different ionic strengths.

This is the peer-reviewed, final accepted version for American Mineralogist, published by the Mineralogical Society of America.
The published version is subject to change. Cite as Authors (Year) Title. American Mineralogist, in press.
DOI: https://doi.org/10.2138/am-2022-8834. http://www.minsocam.org/

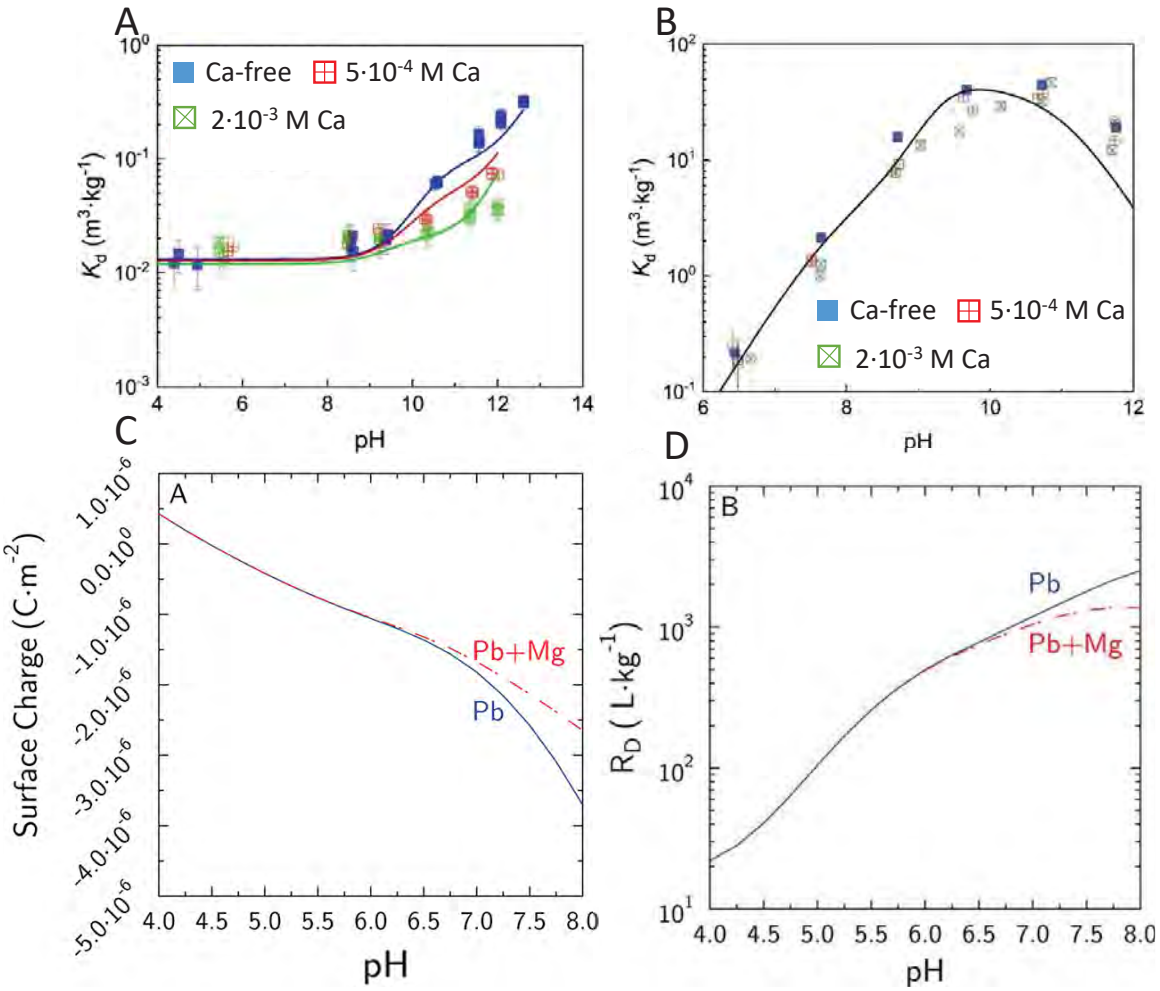

Fig. 8 The competitive adsorption behavior of Ca^{2+} in the presence of competition cations (i.e., Sr^{2+}, Ni^{2+}, and Pb^{2+}) on Mt edge surfaces. (A) Sr^{2+} adsorbed onto Na-Mt in the presence and absence of Ca^{2+}, (B) Ni^{2+} adsorbed onto Na-Mt in the presence and absence of Ca^{2+}. (Adapted with permission from Sugiura et al., (2021), Applied Clay Science, 200, 105910. Copyright 2021, with permission from Elsevier.). (C) Effect of the addition of Mg^{2+} on (C) Mt edge surface charge and (D) Pb^{2+} adsorption on edge surface. (Adapted with permission from Orucoglu et al., (2022), ACS Earth and Space Chemistry, 6, 144-159. Copyright 2022 American Chemical Society.).

This is the peer-reviewed, final accepted version for American Mineralogist, published by the Mineralogical Society of America.
The published version is subject to change. Cite as Authors (Year) Title. American Mineralogist, in press.
DOI: https://doi.org/10.2138/am-2022-8834. http://www.minsocam.org/

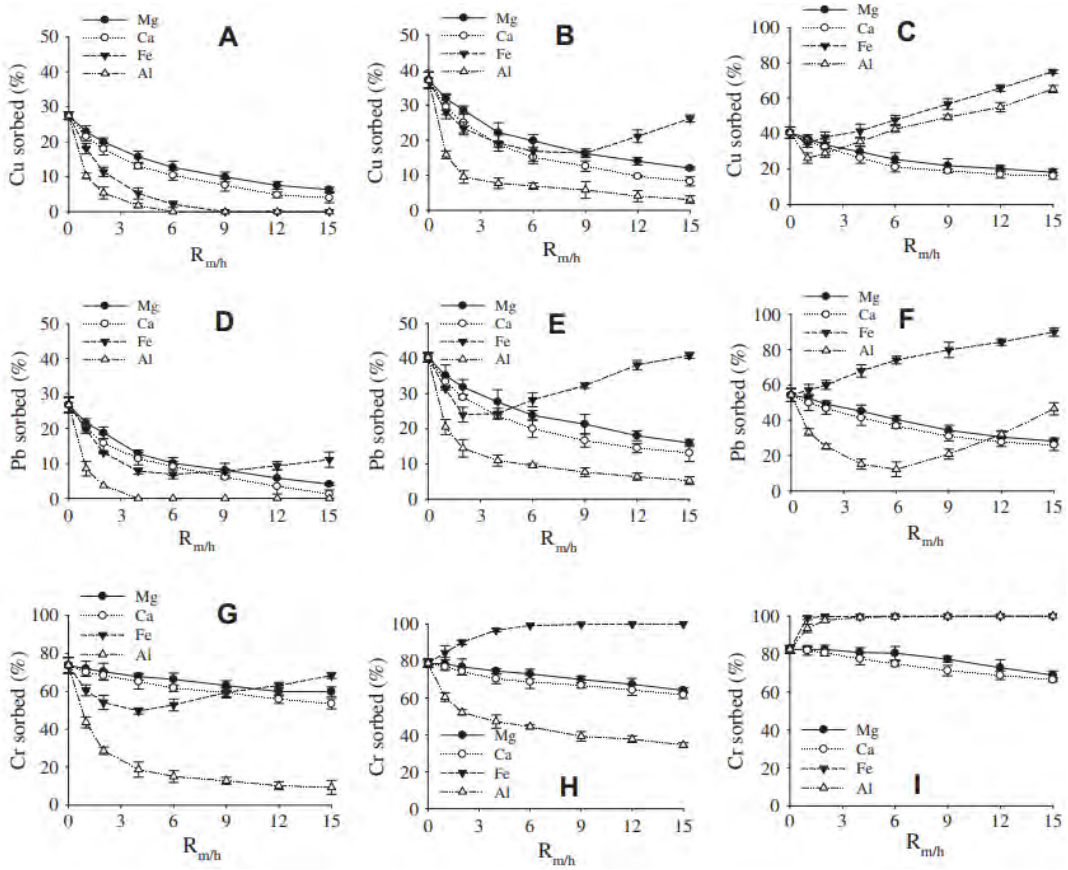

Fig. 9 Effect of competing cations (Al^{3+}, Fe^{3+}, Ca^{2+} and Mg^{2+}) on the adsorption of heavy metal pollutants (Cu^{2+}, Pb^{2+} and Cr^{2+}) by Na-Mt with increasing concentration ratio of competing cations to target metal ($R_{m/h}$) from 0 to 15: (A) Cu at pH 3.5, (B) Cu at pH 4.5, (C) Cu at pH 5.5, (D) Pb at pH 3.5, (E) Pb at pH 4.5, (F) Pb at pH 5.5, (G) Cr at pH 3.5, (H) Cr at pH 4.5, and (I) Cr at pH 5.5. (Adapt with permission from Zhu et al., (2011), Chemosphere, 84, 484-489. Copyright 2011, with permission from Elsevier.).

This is the peer-reviewed, final accepted version for American Mineralogist, published by the Mineralogical Society of America.
The published version is subject to change. Cite as Authors (Year) Title. American Mineralogist, in press.
DOI: https://doi.org/10.2138/am-2022-8834. http://www.minsocam.org/

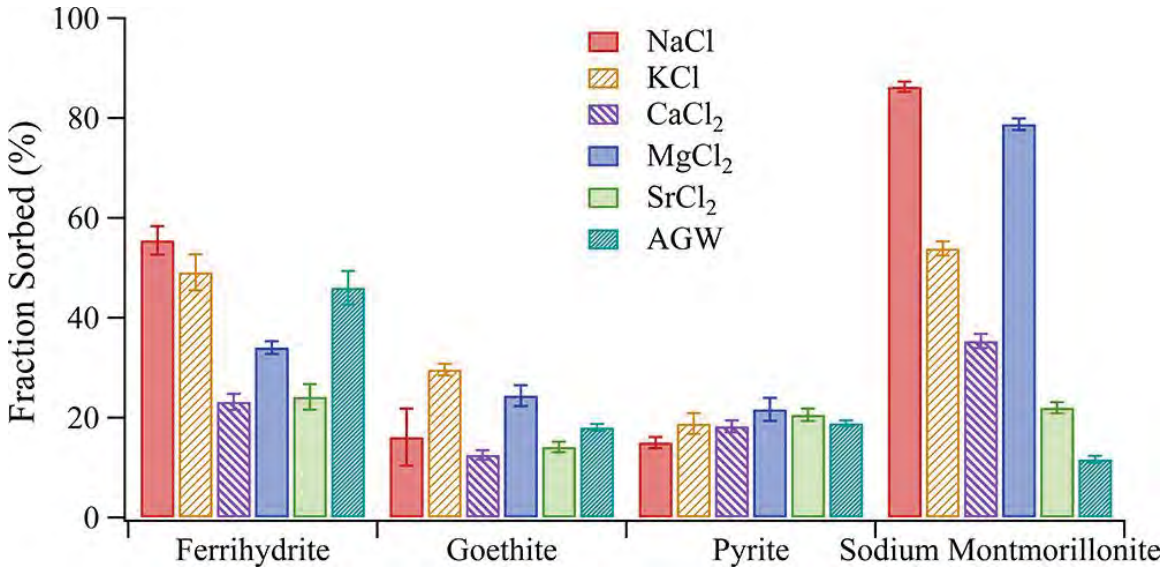

Fig. 10 Impact of competing cations on Ra^{2+} adsorption. The concentrations of NaCl, KCl, $CaCl_2$, $MgCl_2$, and $SrCl_2$ are all 10 mM, AGW (artificial groundwater) is composed of elements, such as Na (5 mM), K (2 mM), Mg (0.5 mM), Ca (0.5 mM), Sr (0.0001 mM), and Cl (9 mM). (Adapted with permission from Chen and Kocar, (2018), Environmental Science & Technology, 52, 4023-4030. Copyright 2018 American Chemical Society.).

This is the peer-reviewed, final accepted version for American Mineralogist, published by the Mineralogical Society of America.
The published version is subject to change. Cite as Authors (Year) Title. American Mineralogist, in press.
DOI: https://doi.org/10.2138/am-2022-8834. http://www.minsocam.org/

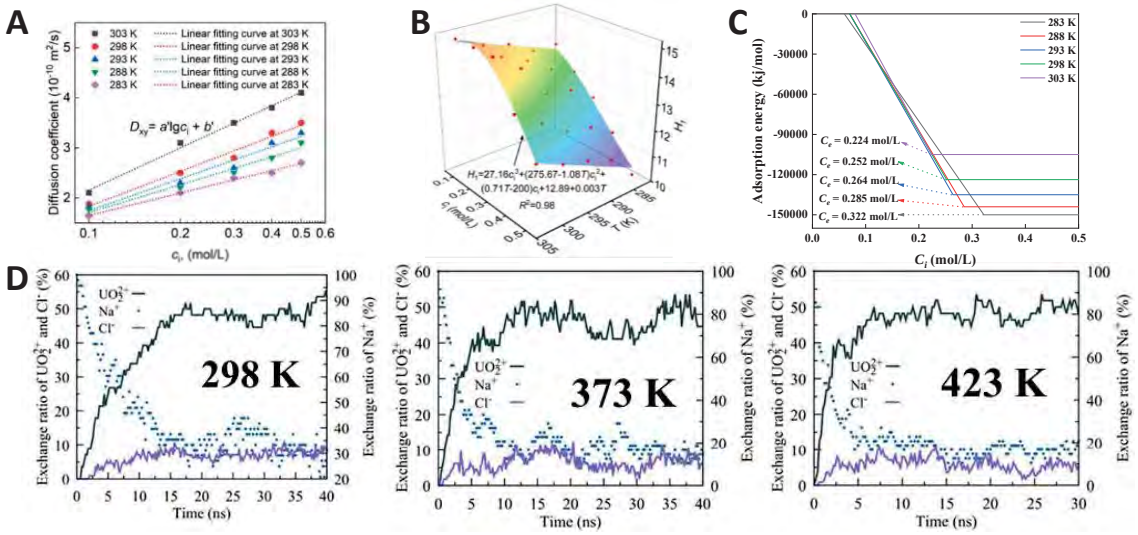

Fig. 11 Temperature dependency of the cation adsorption processes. (A) Effect of temperature on (A) diffusion coefficient, (B) hydration state, and (C) the adsorption energy of Pb^{2+} ion (C_i: initial Pb^{2+} concentration; H_1: first peak value of radial distribution function curve of Pb^{2+} to water oxygen; C_e: maximum initial Pb^{2+} concentration identified by adsorption energy) (Adapted with permission from Du et al., (2022), Environmental Research, 209, 112817. Copyright 2022, with permission from Elsevier.). (D) Adsorption behavior of metal cations on Mt basal surface at 298, 373, and 423 K. (Adapted with permission from Zhang et al., (2022), Applied Clay Science, 226, 106579. Copyright 2022, with permission from Elsevier.).

This is the peer-reviewed, final accepted version for American Mineralogist, published by the Mineralogical Society of America.
The published version is subject to change. Cite as Authors (Year) Title. American Mineralogist, in press.
DOI: https://doi.org/10.2138/am-2022-8834. http://www.minsocam.org/

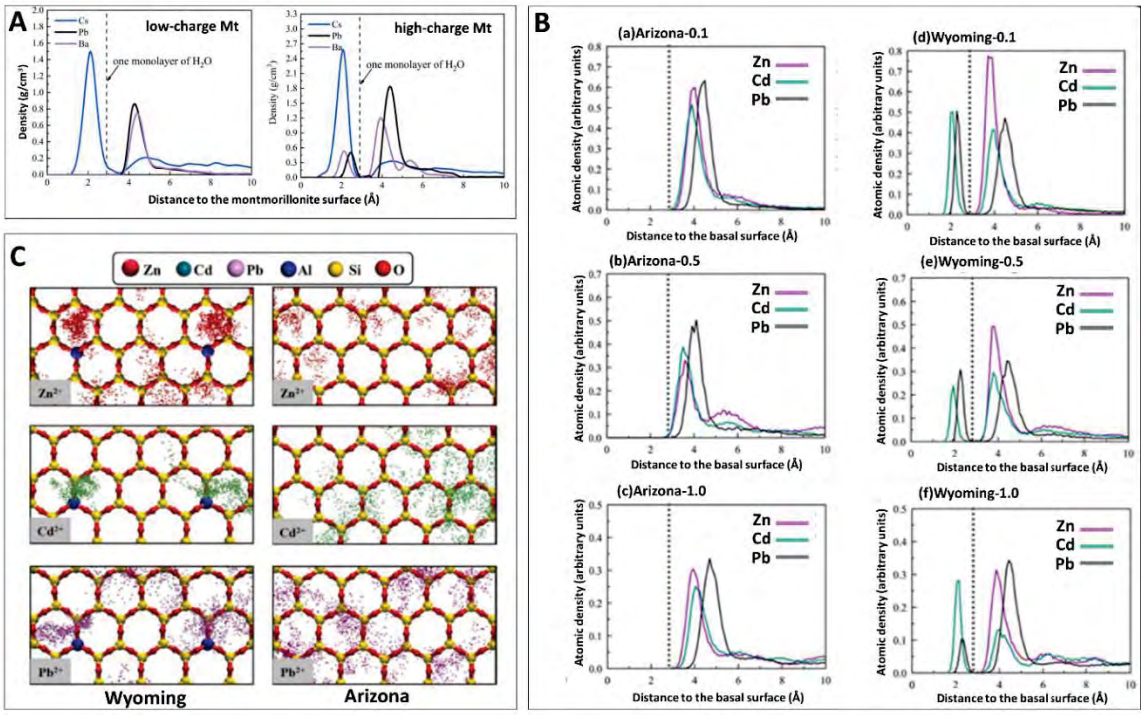

Fig. 12 The influence of layer charge density and location on the cation exchange process. (A) The density distributions of Pb^{2+}, Ba^{2+}, and Cs^{+} and water oxygen atoms on surface basal plane (Adapted with permission from Zhang et al., (2023), Colloids and Surfaces A: Physicochemical and Engineering Aspects, 657, 130553. Copyright 2023, with permission from Elsevier.). (B) Atomic density profiles of Zn^{2+}, Cd^{2+}, and Pb^{2+} cations along the direction perpendicular to Arizona and Wyoming Mt basal surfaces and (C) Time-evolution trajectories of the adsorbed heavy metal cations at basal surfaces of Arizona and Wyoming Mt. (Adapted with permission from Liu et al., (2021), Journal of Hazardous Materials, 416, 125976. Copyright 2021, with permission from Elsevier.).

This is the peer-reviewed, final accepted version for American Mineralogist, published by the Mineralogical Society of America.
The published version is subject to change. Cite as Authors (Year) Title. American Mineralogist, in press.
DOI: https://doi.org/10.2138/am-2022-8834. http://www.minsocam.org/

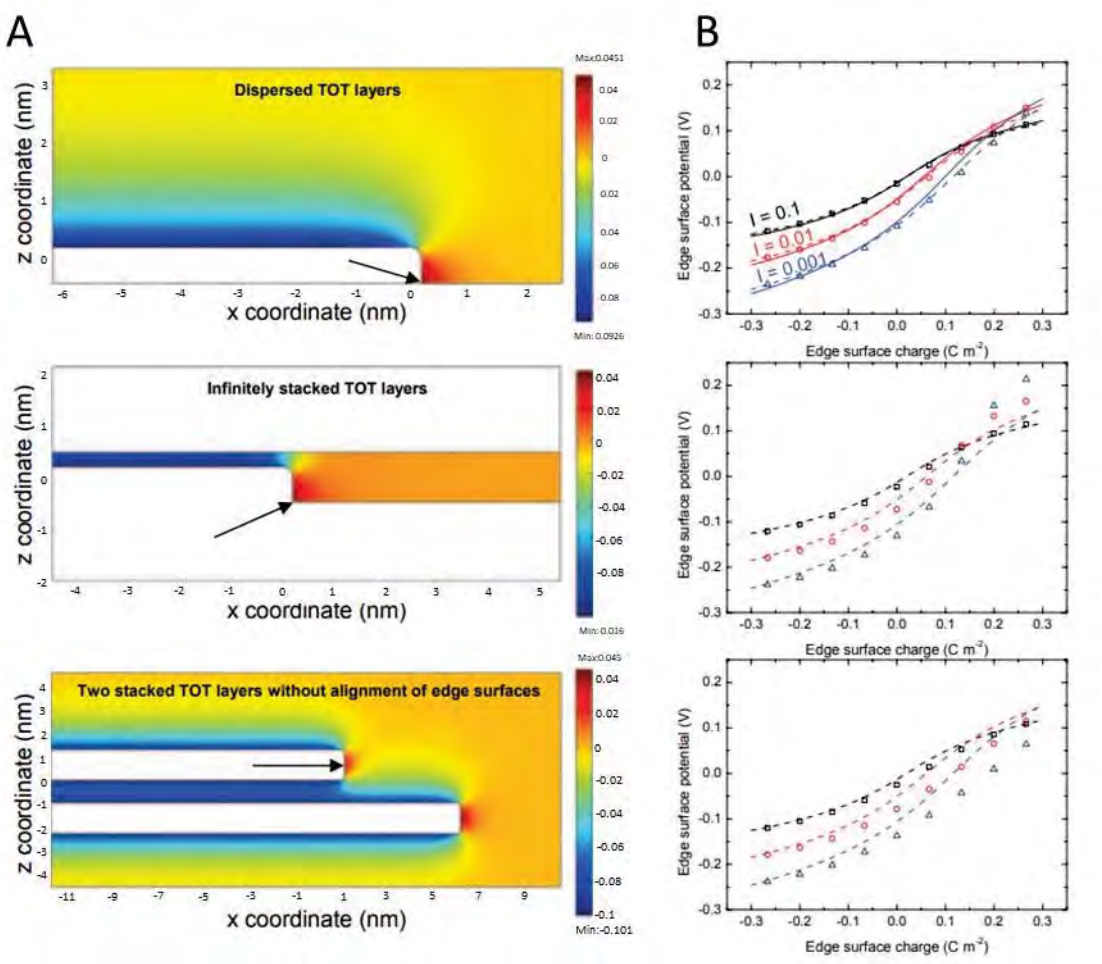

Fig. 13 Electrostatic spillover effect of Mt layer related to the stacking modes and ionic strengths. (A) 2D geometry considered for solving the Poisson-Boltzmann equation (zoom on the edge surface region) in three different geometries. (B) The edge potential as a function of edge charge for three ionic strengths (0.001, 0.01, and 0.1) at the arrow position in panel A. (Adapted with permission from Tournassat et al., (2013), American Journal of Science, 313, 395-451. Copyright 2013, with permission from American Journal of Science.).